Journal of Aerosol Science 42 (2011) 693–724

Contents lists available at ScienceDirect

Journal of Aerosol Science

journal homepage: www.elsevier.com/locate/jaerosci

Review

Modelling inhaled particle deposition in the human lung—A review

Werner Hofmann*

Division of Physics and Biophysics, Department of Materials Research and Physics, University of Salzburg, 5020 Salzburg, Austria

ARTICLE INFO

Article history:
Received 26 July 2010
Received in revised form
28 May 2011
Accepted 30 May 2011
Available online 12 June 2011

Keywords:
Human lung
Inhalation
Aerosol
Deposition
Modelling

ABSTRACT

Particle deposition in the human respiratory tract is determined by biological factors such as lung morphology and breathing patterns, and physical factors such as fluid dynamics, particle properties, and deposition mechanisms. Current particle deposition models may be grouped into two categories referring to the region of interest in the lung, i.e. either deposition in the whole lung (whole lung models), or deposition in a localized region of the lung (local scale models). In whole lung models, particle deposition in individual airways is computed by analytical equations for particle deposition efficiencies and specific flow conditions (analytical models). The present review focuses upon the philosophy of different conceptual whole lung models to determine deposition in bronchial and acinar airway generations, and to compare the deposition patterns predicted by these models. Since any modelling approach requires validation by comparison with the available experimental evidence, predicted deposition data are compared with published experimental data in human subjects. This comparison indicates that, at least during the writing of this review, deposition models can be validated only for total and, to some extent, for regional deposition. In local scale models, particle transport and deposition equations are solved by Computational Fluid and Particle Dynamics (CFPD) methods (numerical models), providing information on particle deposition patterns within selected structural elements of the lung, e.g. bronchial bifurcations. In this review, however, only their potential contribution to improve upon current analytical whole lung models will be considered.

Contents

* Tel.: +43 662 8044 5705; fax: +43 662 8044 150.
E-mail address: Werner.Hofmann@sbg.ac.at

0021-8502/$ - see front matter © 2011 Elsevier Ltd. All rights reserved.
doi:10.1016/j.jaerosci.2011.05.007

1. Introduction

At present, direct experimental *in situ* determination of particle deposition in human subjects is limited to total deposition, measured as the difference between inhaled and exhaled aerosol concentrations in a single breath, either inhaling through the mouth or the nose, for a wide range of particle sizes and flow rates (e.g. Heyder et al., 1986; International Commission on Radiological Protection (ICRP), 1994). Regional, i.e. extrathoracic, bronchial and acinar deposition (ICRP, 1994) as a function of particle size and flow rate can only be derived indirectly via subsequent retention measurements of radiolabelled aerosols (e.g. Heyder et al., 1986; ICRP, 1994) or from the analysis of serial bolus deposition data (Kim & Hu, 1998; Kim & Jaques, 2000). Recent measurements of the deposition of inhaled narrow aerosol boli injected into different volumetric lung depths (Brand et al., 1997; Heyder et al., 1988; Choi & Kim, 2007) or the three-dimensional reconstruction of radiolabelled aerosols by hemispherical shells in Single Photon Computed Tomography (SPECT) (Fleming et al., 1995, 2000) also provide some information on particle deposition in specified groups of airways or airway generations. Additional experimental information about particle deposition in individual airways or airway generations can be obtained from measurements in airway casts and airway models, restricted to large bronchial airways for experimental reasons (Cohen et al., 1990; Martonen, 1983; Oldham et al., 1997). Finally, local deposition patterns within bronchial airway bifurcations have been measured in single and multiple bifurcation models (Kim & Iglesias, 1989; Kim & Fisher, 1999).

Nevertheless, there are several good reasons for modelling particle deposition in the human respiratory tract. The two most important reasons are:

(1) Direct experimental determination of particle deposition in human subjects is limited to total deposition, and, with less accuracy, to regional deposition. However, health risk assessment and aerosol therapy for inhaled particles requires information on local deposition patterns within the lungs. For example, lung carcinomas occur preferentially in the bronchial airways, which imply that we need information on deposition fractions in different bronchial airway generations.
(2) Experimental data refer to specific human subjects and defined inhalation conditions, such as lung volume, particle size, and breathing parameters. However, particle deposition is needed for all members of the population, ranging from children to the elderly, where experimental studies are either forbidden due to ethical considerations or are not feasible for health reasons, and for all particle sizes and breathing conditions.

Thus, particle deposition modelling is a matter of necessity and not a matter of fashion or personal preference. The objectives of this review paper on particle deposition in the whole lung are (i) to discuss the primary physical and biological factors determining particle deposition; (ii) to review the present state of the art in aerosol deposition modelling for the whole lung; (iii) to compare deposition fractions and patterns predicted by different models; (iv) to compare model predictions to the currently available experimental evidence; and, finally; (v) to evaluate the contributions of Computational Fluid and Particle Dynamics (CFPD) models to whole lung deposition calculations. Since research on CFPD models has expanded substantially in recent years, these models deserve a separate review and will thus not be included in this review due to limitations of space.

2. Factors determining particle deposition

Modelling particle deposition in the human lung is an attempt "to solve a physical problem in a biological system by applying mathematical methods". Since this requires information about physics, biology and mathematics, particle deposition modelling is a truly multidisciplinary task. Biological factors include the lung morphology, which defines the airway geometry of a system of cylindrical airways, and respiratory parameters, which determine air flow and velocities of particles entrained in the airstream. Physical factors are the fluid dynamics of the inhaled air volume, which determine airflow patterns throughout the lung, particle properties and physical particle deposition mechanisms, which allow the calculation of deposition fractions in specific airway generations.

Mathematical modelling of aerosol deposition in the human lung requires idealizing assumptions regarding the effects of such physical and biological factors on particle deposition. These assumptions must satisfy two conditions: (1) they must be as anatomically and physiologically realistic as possible, and (2) they must permit analytical or numerical solutions of the equations governing air flow, particle transport, and deposition. These two intimately connected conditions imply that more realistic morphometric and physiological models require more sophisticated mathematical modelling techniques.

2.1. Morphometric lung models

One of the major differences among currently available models of inhaled particle deposition in the whole lung is the application of different morphometric lung models, ranging from regional compartment models to detailed bronchial and acinar airway structures. Hence the different morphometric lungs models will be described in more detail.

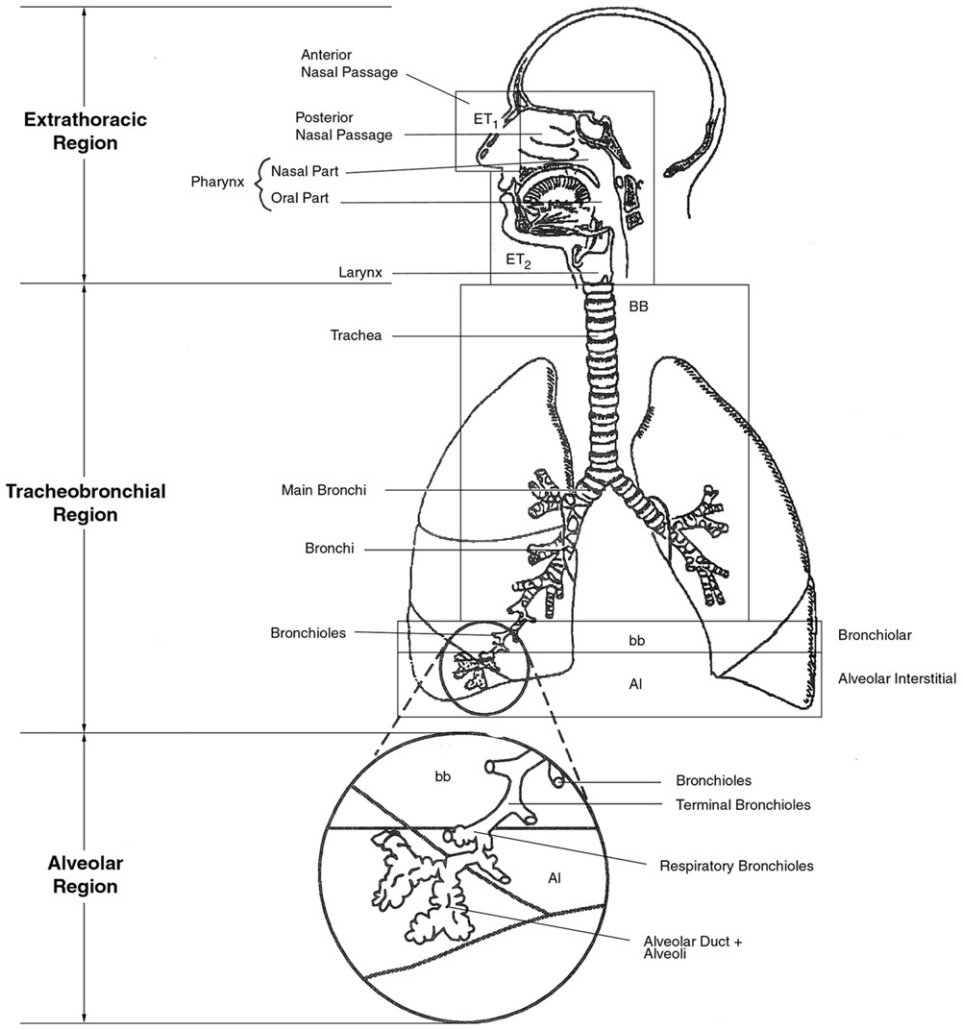

Fig. 1. Illustration of the major anatomical regions of the human respiratory tract (ICRP, 1994). *Abbreviations*: ET_1: anterior nasal passages; ET_2: posterior nasal passages, naso-oropharynx, and larynx; BB: bronchial region, including trachea and bronchi; bb: bronchiolar region consisting of bronchioles and terminal bronchioles; AI: alveolar-interstitial region, consisting of respiratory bronchioles, and alveolar ducts and sacs surrounded by alveoli.

The human respiratory tract is commonly divided into three major compartments (ICRP, 1994): (i) the extrathoracic (ET) region, extending from the nose or the mouth to the entrance of the trachea, (ii) the tracheobronchial (TB) region, ranging from the trachea to the terminal bronchioles, and (iii) the acinar (A) or alveolar-interstitial (AI) or pulmonary (P) region, where gas exchange takes place between air and blood via the alveoli (*note*: the term acinar will be consistently used throughout the course of this paper, although AI and P are frequently used in the literature). Morphometric lung models always refer to the lung (thoracic region), consisting of the TB and A compartments, while the ET region is considered merely as a filter, which determines the fraction of particles actually reaching the lung. A detailed schematic description of the human respiratory tract is shown in Fig. 1 (ICRP, 1994).

Modelling particle deposition in the human lung requires a geometric description of the branching airway structure. In all morphometric lung models, the parent airway branches into two daughter airways at each bifurcation, either in a simplified symmetric fashion (ICRP, 1994; Weibel, 1963; Yeh & Schum, 1980) or considering the experimentally observed asymmetric branching scheme (Horsfield & Cumming, 1968; Koblinger & Hofmann, 1985). While conductive airways in the TB region are represented by straight cylindrical tubes of given length and diameter, alveoli attached to the respiratory airways in the A region can be approximated by spherical volumes with different levels of truncation (Hansen & Ampaya, 1975). The airway topology, i.e. the location of individual airways within the lung relative to the trachea, is generally characterized by an assigned airway generation number, typically starting with generation 0 (ICRP, 1994; Weibel, 1963) or 1 (Koblinger & Hofmann, 1985; Yeh & Schum, 1980) for the trachea. Consequently, the branching network of the human lung is represented by a serial succession of cylindrically-shaped airway generations (ICRP, 1994; Weibel, 1963; Yeh & Schum, 1980) or by a sequence of Y-shaped airway bifurcations (Koblinger & Hofmann, 1985). For example, Fig. 2 illustrates the network of bifurcating bronchial airways of the human lung branching off the trachea, based on the morphometric measurements by Raabe et al. (1976).

The two most extensive morphometric data sets of the bronchial tree geometry have been provided by Weibel (1963) and Raabe et al. (1976). For modelling purposes, these morphometric data were subsequently utilized to define bronchial tree models, the Weibel (1963) model A, later modified by Haefeli-Bleuer and Weibel (1988), and the Yeh and Schum (1980) typical path model. Other models of the bronchial tree were published by Horsfield and Cumming (1968) (*note*: this asymmetric branching model differs from all other models as airway generations are counted upward, ending at the trachea as generation 25), Phalen et al. (1985), and the model proposed by James (1988), adapted from the models of Weibel (1963), Yeh and Schum (1980), and Phalen et al. (1985).

In recent years, Magnetic Resonance Imaging (MRI) and Computer Tomography (CT) techniques made it possible to determine the bronchial airway geometry of individual subjects, restricted however to large bronchial airways due to the limited spatial resolution (e.g. Takano et al., 2006). These anatomically most realistic airway models are currently used for

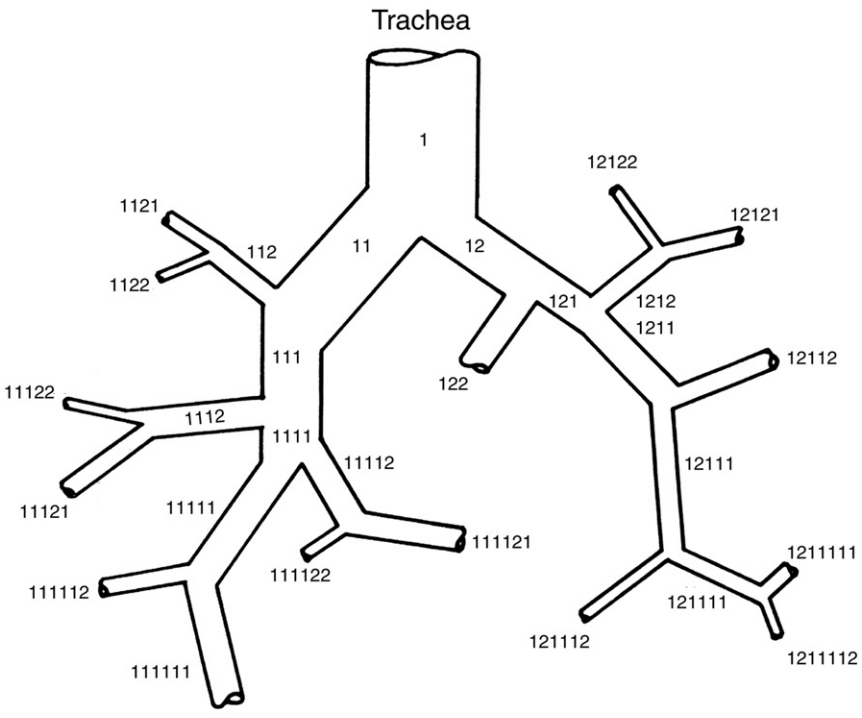

Fig. 2. Schematic description of the upper tracheobronchial tree (Raabe et al., 1976). The binary identification number system used for the tracheobronchial airways starts with 1 for the trachea and designates major and minor branches with 1 and 2, respectively.

Computational Fluid and Particle Dynamics (CFPD) calculations in selected anatomical regions, such as large bronchial airways or nasal and oral passages rather than for the construction of whole lung models.

In the measurements of Raabe et al. (1976), the structural parameters of the bronchial tree, i.e. diameters, lengths, branching and gravity angles, were recorded for the trachea and all bronchial airways down to about generation 10, but only 10–25% of bronchiolar airways ending at terminal bronchioles were measured. For the acinar airway generations, consisting of alveolar ducts and sacs and alveoli, no data were provided in this morphometric study due to size constraints. Thus the problem arises of how to complete the bronchiolar airway structure and to define the structure of the acinar region.

The simplest and computationally most convenient method is to calculate the arithmetic means for all structural parameters of the bronchiolar airway system, where only a fraction of airways was actually measured, assuming that the measured fraction is also representative of the airway geometry of the missing airways. This averaging procedure leads to the construction of symmetric deterministic lung models (e.g. ICRP, 1994; Weibel, 1963; Yeh & Schum, 1980). In these symmetrically branching deterministic lung models, each airway in a given airway generation has identical linear dimensions and consequently the same pathlength from the trachea. Thus these models are commonly called "typical path models" as all pathways of inhaled particles are identical during inhalation as well as exhalation.

Despite the simplicity and computational convenience of these deterministic symmetric lung models, they cannot reproduce, by definition, the asymmetry of the airway branching pattern (see Fig. 2). Thus, based on the morphometric measurements of Raabe et al. (1976), Yeh and Schum (1980) proposed a deterministic five-lobe typical path model with variable pathlengths among the five lobes, but symmetric branching within each lobe.

Instead of using average values for the bronchial airways, Asgharian et al. (2001) proposed a deterministic asymmetric or "multiple-path" model, based on the Raabe et al. (1976) data for each completely measured bronchial airway generation. Since a complete description of the bronchiolar airways of the human lung is presently not available, 10 (later extended to 50) asymmetric, structurally different multiple-path bronchial airway models were constructed on the basis of the stochastic lung model (Asgharian et al., 2001; Hofmann et al., 2002).

Stochastic lung models offer the possibility to extend the measured data for the specific lungs analysed by Weibel (1963) or Raabe et al. (1976) to the adult population at large. The first step towards a stochastic airway model was attempted by Yu et al. (1979) and Yu and Diu (1982), who simulated inter-subject differences in airway dimensions by two random scaling factors for tracheobronchial and acinar air volumes on the basis of the deterministic, symmetric lung model A of Weibel (1963). The stochastic model proposed by Goo and Kim (2003) considers random variations of the airway morphology by simulating the path of an infinitesimal air volume through the symmetric model A of Weibel (1963).

In the fully asymmetric stochastic multiple path model developed by Koblinger and Hofmann (1985, 1990) and Hofmann and Koblinger (1990), airway diameters, lengths, branching and gravity angles in bronchial and bronchiolar airways (Raabe et al., 1976) were statistically analysed in terms of frequency distributions, e.g. diameters and lengths were approximated by lognormal distributions, and correlations among several parameters, e.g. between parent and daughter cross-section. Thus bronchiolar airways were completed by assuming that the parameter distributions and correlations in the missing airways are the same as those in the measured airways, although not their absolute values. The morphometrically observed branching asymmetry and variability of airway dimensions (see Fig. 2) leads to highly variable pathlengths from the trachea to a given generation. For example, the first respiratory airways of the acinar region were already found in airway generation 12, while the last terminal bronchiole was still measured in generation 21. Despite this variability, the average number of tracheobronchial airway generations is between 16 and 17, consistent with the symmetric morphometric models of Weibel (1963) and Yeh and Schum (1980).

The morphometric data base for the acinar region is even smaller than for the tracheobronchial region. First measurements were reported by Hansen and Ampaya (1975), later used in the ICRP (1994) Human Respiratory Tract Model, and by Weibel (1963), incorporated into his model A. Yeh and Schum (1980) defined a symmetric acinar airway model based on a limited number of morphometric data, assumptions on the total number of alveoli and the total lung capacity (TLC), and several theoretical considerations. Thus, identical acini are attached to each terminal bronchiole. This acinar structure was also assumed by Asgharian et al. (2001) in a version of the multiple path model.

As of today, the most extensive data set of acinar airways was supplied by Haefeli-Bleuer and Weibel (1988). Average values for acinar airway diameters and lengths were implemented into a revised Weibel model (Haefeli-Bleuer & Weibel, 1988), thereby reducing the originally published number of tracheobronchial airway generations. In the stochastic lung model (Koblinger & Hofmann, 1990), these data were again statistically analysed to define a stochastic, acinar geometry, which considers the additional variability in the number of acinar airway generations along a given pathway, varying between 6 and 12 airway generations with an average number of 9, and the linear dimensions in each airway. This stochastically generated acinar geometry was also incorporated into a later version of the multiple path model (Asgharian et al., 2001).

Different approaches have been proposed for the incorporation of alveoli into acinar airway models. The methods commonly used in symmetric deposition models are that of effective channel diameters, obtained by enlarging the diameters of alveolar ducts by the volume of adjacent alveoli (e.g. Martonen, 1982), or of an effective alveolar volume per generation in the case of one-dimensional cross-section models (Taulbee & Yu, 1975; Taulbee et al., 1978). In the stochastic lung model (Koblinger & Hofmann, 1990) and the serial bolus model (Choi & Kim, 2007), deposition in single alveoli (Koblinger & Hofmann, 1990) is computed for each respiratory airway generation, assuming that all alveoli are of the same size and shape (truncated spherical shape) (Hansen & Ampaya, 1975), multiplied by the distribution of the number of alveoli per generation provided by Weibel (1963).

Table 1
Airway parameters of the typical path model of the human lung proposed by Yeh and Schum (1980).

n	N	D (cm)	L (cm)	θ (deg.)	φ (deg.)	S (cm^2)	V (cm^3)	$\sum V$ (cm^3)
1	1	2.01	10.0	0	0	3.17	31.73	31.73
2	2	1.56	4.36	33	20	3.82	16.67	48.40
3	4	1.13	1.78	34	31	4.01	7.14	55.54
4	8	0.827	0.965	22	43	4.30	4.15	59.69
5	16	0.651	0.995	20	39	5.33	5.30	64.98
6	32	0.574	1.01	18	39	8.28	8.36	73.35
7	64	0.435	0.890	19	40	9.51	8.47	81.81
8	128	0.373	0.962	22	36	13.99	13.46	95.27
9	256	0.322	0.867	28	39	20.85	18.07	113.34
10	512	0.257	0.667	22	45	26.56	17.72	131.06
11	1024	0.198	0.556	33	43	31.53	17.53	148.59
12	2048	0.156	0.446	34	45	39.14	17.46	166.05
13	4096	0.118	0.359	37	45	44.79	16.08	182.13
14	8192	0.092	0.275	39	60	54.46	14.98	197.10
15	16,384	0.073	0.212	39	60	68.57	14.54	211.64
16[a]	32,768	0.060	0.168	51	60	92.65	15.57	227.21
17	65,536	0.054	0.134	45	60	150.09	20.11	247.32
18	131,072	0.050	0.120	45	60	257.36	30.88	278.20
19	262,144	0.047	0.092	45	60	454.81	41.84	320.04
20	524,288	0.045	0.080	45	60	833.84	66.71	386.75
21	104,8576	0.044	0.070	45	60	1594.39	111.61	498.36
22	209,7152	0.044	0.063	45	60	3188.78	200.89	699.25
23	419,4304	0.043	0.057	45	60	6090.97	347.19	1046.44
24	838,8608	0.043	0.053	45	60	12,181.95	645.64	1692.08
25[b]	3×108	0.030	0.025	45	60	–	3871.80	5563.88

n=generation number; N=number of airways; D=airway segment diameter; L=airway segment length; θ=branching angle; φ=gravity angle with 90° corresponding to a horizontal tube; S=cross-sectional area; V=volume; $\sum V$=cumulative volume.
[a] Terminal bronchioles.
[b] Alveoli.

To illustrate the structure of whole lung airway models, the number of airways, diameters, lengths, branching and gravity angles, and related parameters of the typical path model of Yeh and Schum (1980) are compiled in Table 1. This particular lung geometry model was selected because it is based on the morphometric measurements of Raabe et al. (1976), which also form the basis of the stochastic lung model (Koblinger & Hofmann, 1985) and the asymmetric multiple path model (Asgharian et al., 2001). Since it is a deterministic symmetric airway model, all airway generations from 1 (trachea) to 16 (terminal bronchioles) form the bronchial tree, while acinar airways range from generation 17 (first respiratory airway) to generation 24 (alveolar sac), and all alveoli are lumped together in generation 25. The listed airway diameters and lengths refer to a total lung volume of about 5500 ml.

For modelling purposes, however, these airway diameters and lengths must be modified by applying two scaling procedures. As the measured bronchial airway dimensions in the Raabe et al. (1976) study reportedly refer to total lung capacity (TLC) (Yeh & Schum, 1980), all bronchial airway diameters and lengths have to be scaled down to a standard functional residual capacity (FRC) of 3300 ml for an adult male (or 2680 ml for an adult female) (ICRP, 1994), commonly by a constant scaling factor defined by the cube root of the ratio of standard FRC to TLC. The same scaling procedure can be applied for the extrapolation from the standard FRC to an individual FRC, assuming similar lung structures (Hofmann et al., 2002). Upon inspiration of a defined tidal volume V_T, each airway, except for trachea and main and lobar bronchi, is assumed to expand at the same rate in a linear fashion until reaching a lung volume of $FRC+V_T$ at the end of inspiration, and likewise to contract to FRC at the end of expiration. For deposition calculations, the roughly linearly increasing and decreasing lung volume can be approximated by an average constant lung volume of $FRC+V_T/2$, to which airway diameters and lengths are finally rescaled to.

2.2. Respiratory physiology

The main physiological factors determining particle deposition are the breathing frequency f, i.e. the number of breaths per minute, and the tidal volume V_T, which is the volume inhaled during a single breath (their product is termed respiratory minute volume $RMV=V_T \times f$). Both breathing frequency and tidal volume depend on the physical activity of a person. Standardized values for resting (sleeping), sitting awake, light exercise, and heavy exercise for men and women and children of different ages are listed in the ICRP (1994) report. Additional breathing parameters for modelling purposes are the inspiration, expiration and breath-hold times and the time dependence of the lung volume during both breathing phases, approximated either by a linear or a sine function (*note*: calculations have demonstrated that the exact shape of this function hardly affects resulting deposition fractions). The corresponding physical parameters determining particle deposition are the particle velocity u in a given airway, which decreases when penetrating deeper into the lung.

Alternative parameters related to the particle velocity are the inspiratory flow rate Q, the air volume inhaled during the inspiration phase (tidal volume/inspiration time), or the residence time τ within a given airway.

2.3. Fluid dynamics

The transport of inhaled particles through the whole lung is based on the fundamental principle that particles contained in a given air volume travel with the same velocity as that air volume (“convective transport”). For small particles, however, the axial velocity of these particles may be slightly higher or smaller than the velocity for the convective transport (“axial diffusion”), which can be expressed by an effective diffusion coefficient, depending on axial flow velocity, particle diffusion coefficient and airway diameter (Scherer et al., 1975; Hofmann et al., 2008; Lee et al., 2000; Lee & Lee, 2001). The effect of axial dispersion is partly responsible for the experimentally observed dispersion of a narrow inhaled aerosol bolus (Brand et al., 1997).

Recent CFD simulations in an alveolar duct model (Butler & Tsuda, 1997; Tsuda et al., 1995, 2008, 2002) as well as laboratory measurements (Tippe & Tsuda, 1999) suggest that flow-induced alveolar mixing, caused by the irreversibility of alveolar flow combined with a stretched and folded pattern of streamlines, can lead to a mixing of the inhaled tidal air with the residual air in the lungs. In whole lung deposition models, alveolar mixing can be considered by an empirical mixing factor, derived from experimental data (Hofmann et al., 2008).

In symmetrically branching typical path models, flow splitting at airway bifurcations is also symmetric within a given generation. In asymmetrically branching lung models, however, flow splitting is commonly assumed to be proportional to the distal lung volume which is supported by either daughter airway (Asgharian et al., 2006; Hofmann et al., 2008). Moreover, differences in ventilation between different topographic regions of the lung, termed asymmetry, i.e. upper vs. lower lobes and left vs. right lung (Cruz, 1991; Milic-Emili et al., 1966), and a sequential filling of different parts of the lung, termed asynchrony, i.e. upper lobes are filled more rapidly at the onset of inspiration than the lower lobes (Grant et al., 1974; Fukuchi et al., 1980), have been observed experimentally. Asymmetric lung ventilation can be modelled by lobe-specific ventilation coefficients and asynchronous ventilation by time-dependent linear functions (Hofmann et al., 2008). Asgharian et al. (2006) compared several models of non-uniform expansion and contraction that account for airway resistance and tissue compliance. Such non-uniform ventilation models play only a minor role for normal breathing in a healthy lung, but may be required for the calculation of hypergravity, high breathing rates, or airway diseases.

Air flow patterns within the lung are determined by a complex interplay of structural features, such as individual airway dimensions and the spatial configuration of the branching network, and ventilatory conditions. Airway fluid dynamics at the whole lung level addresses primarily the question whether the bulk primary motion is laminar or turbulent or whether the primary velocity profiles are flat or parabolic. While most particle deposition models assume developing or fully developed, i.e. laminar parabolic flow in all airway generations, results of experimental and theoretical investigations of air flow patterns suggest that fluid dynamics patterns vary with increasing penetration into the lungs. For example, Martonen (1993) proposed the following fluid dynamics pattern: (1) at the entrance of the trachea, flow is characterized by the action of the laryngeal jet, (2) in the large bronchi, turbulent flow may exist even at small Reynolds numbers because of instabilities induced by the larynx and the cartilaginous rings in the trachea, (3) airflow patterns in the lower bronchial and bronchiolar airways are described by a laminar flow with a uniform or plug velocity profile, reflecting the influence of airway branchings, and (4) in the acinar region, laminar flow is fully developed with a parabolic profile due

Table 2
Compilation of currently used analytical equations for particle deposition efficiencies in human airways.

Physical mechanism	References	Flow characteristics
Diffusion	Cohen and Asgharian (1990)	Laminar developing flow
	Ingham (1975)	Laminar parabolic and uniform flow
	Ingham (1984)	Laminar developing flow
	Martonen (1982)	Laminar parabolic and turbulent flow
	Yeh and Schum (1980)	Laminar parabolic flow
	Yu and Cohen (1994)	Laminar developing flow
Impaction[a]	Cai and Yu (1988)	Laminar parabolic flow
	Chan and Lippmann (1980)	Laminar parabolic flow
	Kim et al. (1994)	Laminar parabolic flow
	Yeh and Schum (1980)	Laminar parabolic flow
	Zhang et al. (1997)	Laminar parabolic flow
Sedimentation	Martonen (1982)	Laminar parabolic and turbulent flow
	Pich (1972)	Laminar parabolic flow in horizontal tubes
	Wang (1975)	Laminar parabolic flow in uphill and downhill tubes
	Yeh and Schum (1980)	Laminar parabolic flow

[a] If deposition by inertial impaction in a given generation is expressed in terms of the Stokes number, some equations refer to the Stokes number in that generation (parent airway), while others refer to the next generation downstream (daughter airway) where impaction actually takes place.

the small velocities in these airways. Upon expiration, laminar flow prevails in all regions, with a uniform profile caused by merging flows at airway bifurcations. Similar fluid dynamics patterns are assumed in other particle deposition models. In most models, laminar flow with a parabolic profile is assumed for all bronchial and bronchiolar airway generations, partly because of simplicity, partly because of consistency with the available particle deposition equations.

Because of the complexity of the airway system, fluid dynamics and particle deposition in analytical whole lung deposition models are treated independently, i.e. particle deposition in individual airways is related to air flow by appropriate analytical equations for particle deposition efficiencies for specified flow conditions (*note*: this separation is no longer necessary in local scale CFPD models). For example, deposition by Brownian motion in cylindrical airways can be described by different equations for laminar, parabolic flow (Ingham, 1975; Martonen, 1982; Yeh & Schum, 1980), laminar uniform flow (Ingham, 1975), and developing laminar flow (Cohen & Asgharian, 1990; Ingham, 1984; Martonen, 1982; Yu & Cohen, 1994) (see Table 2). Thus the assignment of defined flow patterns to specific airway generations determines which analytical deposition equations will be used for particle deposition calculations in the different deposition models.

A detailed description of fluid dynamics principles and applications can be found in related textbooks (Reist, 1993; Hinds, 1999; Friedlander, 2000; Williams & Loyalka, 2000; Finlay, 2001; Baron & Willeke, 2005).

2.4. Particle properties

The deposition of an inhaled particle is governed by its size. The relevant diameter for Brownian diffusion is the mobility equivalent (sometimes also called diffusion equivalent) diameter d_{me}; the appropriate diameter for impaction and sedimentation is the aerodynamic diameter d_{ae} which takes into account the density of a particle relative to unit density. In the case of non-spherical particles, the relationship between the d_{me} (or d_{ae}) of an irregularly shaped particle and its volume equivalent diameter can be described by constant (ICRP, 1994) or dynamic shape factors (Kasper, 1982a; Park et al., 2004; Hofmann et al., 2009).

The effective particle diameter may change upon penetration into the lung, e.g. by hygroscopic growth (Ferron, 1977; Ferron et al., 1993; Martonen et al., 1985; Mitsakou et al., 2005; Robinson & Yu, 1998), or perhaps even by coagulation in case of very high particle concentrations (Mitsakou et al., 2005; Robinson & Yu, 1999). For more information about particle properties, the reader is referred to textbooks (Reist, 1993; ICRP, 1994; Hinds, 1999; Friedlander, 2000; Williams & Loyalka, 2000; Finlay, 2001; Baron & Willeke, 2005). Issues specific to non-spherical particle shape and transport are discussed in various papers by Kasper (1982a, 1982b), Kasper and Shaw (1983), Wen and Kasper (1984), and Kasper and Wen (1984).

2.5. Physical deposition mechanisms

When travelling along an airway, particles will be exposed to different physical mechanisms forcing them to leave the streamlines of the inhaled air volume and eventually depositing on the surrounding airway surfaces. The principal mechanisms acting upon inhaled particles are Brownian diffusion, sedimentation due to gravity, and impaction due to inertial forces. In the case of elongated fibrous particles or chain-like aggregates, interception at airway branching sites must be taken into account as well, and there is experimental evidence for such effects (Scheckman & McMurray, 2011). Additional effects caused by phoretic forces, electrical charge (image forces), or cloud settling may also play a role for specific aerosols and exposure conditions. A general description of physical deposition mechanisms can be found in many textbooks (Reist, 1993; ICRP, 1994; Hinds, 1999; Friedlander, 2000; Williams & Loyalka, 2000; Finlay, 2001; Baron & Willeke, 2005).

This chapter focuses exclusively on particle deposition in human airways, for which quite a number of analytical deposition equations for cylindrical airways has been published during the last decades. It is not the goal of this review to list all deposition equations ever published for deposition in straight or bent cylindrical airways. Detailed information on particle deposition mechanisms and related deposition efficiencies in the human respiratory tract can be found in the open literature. However, Table 2 provides selected references for analytical equations of deposition efficiency which are most widely used in current particle deposition models.

The complexity of the nasal and oral geometry has so far not permitted the derivation of analytical deposition equations as was possible for the cylindrical airways. Semi-empirical equations have been derived by fitting experimental data obtained in human volunteers or airway casts. For example, Cheng et al. (1996) and Cheng (2003) expressed the deposition efficiencies for nasal and oral inhalation and exhalation for two size regimes as a function of Stokes number (for large particles) and the product of diffusion coefficient D and flow rate Q (for small particles). Other semi-empirical equations, based on different sets of experimental data, were reported by Kesavanathan and Swift (1998), Grgic et al. (2004), and Garcia et al. (2009).

The magnitude of each deposition mechanism in lung airways varies with particle parameters (diameter and density), morphometric parameters (airway radius, branching angle and gravity angle), and breathing parameters (residence time or particle velocity). For illustrative purposes, a few examples are listed below.

(1) Impaction is most effective in upper airway generations, where air and particle velocities are higher than in the peripheral region of the lung. By the same token, particles in the alveolated region of the lung are preferentially

deposited by diffusion and sedimentation due to smaller velocities and hence longer residence times. The relevant particle diameter for inertial effects is the aerodynamic diameter.

(2) Small particles, say below 0.5 μm, are deposited primarily by Brownian diffusion (characterized by the mobility equivalent diameter), while deposition by inertial impaction and sedimentation prevails for larger particles, producing the typical U-shape of the total deposition curve which is well known for air filters of any kind.

(3) Slow breathing is most effective for diffusion and sedimentation due to longer residence times, whereas impaction is higher for fast breathing due to higher particle velocities.

(4) Because of the inverse relationship between deposition and airway diameter, deposition efficiencies for all three deposition mechanisms are higher in smaller acinar airways than in larger bronchial airways.

Since a variety of deposition equations for diffusion, impaction and sedimentation have been published (see Table 2), the question arises which equations are the most realistic ones on biological and physical grounds; or, taking a more pragmatic approach, which ones give the best agreement with experimental data on total and regional deposition. Although different deposition equations do produce different generational deposition fractions when incorporated in different models (e.g. Asgharian et al., 2001), no major differences in total deposition fractions have been observed. The choice of a specific set of deposition equations may therefore not be a critical issue, at least not for total and regional deposition.

For deposition calculations, deposition probabilities or efficiencies for each deposition mechanism are first determined independently from each other, and then combined for the simultaneous action of diffusion, inertia, gravity and interception (*note*: this separation is no longer necessary for local scale CFPD models). The total deposition efficiency is then given by the sum of the single deposition efficiencies minus their cross products, assuming that the individual deposition mechanisms are mutually exclusive (Goo & Kim, 2003). Only if one deposition mechanism dominates, e.g. diffusion for nanometre-sized particles, or all deposition efficiencies are small, e.g. in the minimum of the total deposition curve, can the total deposition efficiency be approximated by a linear combination of the individual deposition efficiencies as the cross products become negligibly small.

3. Modelling concepts

From a modelling perspective, current particle deposition models may be grouped into four categories. The first two categories refer to the region of interest in the lung, i.e. either deposition in the whole human lung or respiratory tract (i.e. including the head region) or in selected regions of the lung, e.g. the tracheobronchial region or a given airway generation (whole lung approach), or deposition in a localized region of the lung, comprising a few airways, such as single or multiple airway bifurcations (local scale approach). The other two categories refer to the transport and deposition of inhaled particles, i.e. they either consider the fate of an individual particle (Lagrangian approach) or the fate of a population of particles, characterized by the number or mass concentration (Eulerian approach). All combinations of whole lung, local scale, Lagrangian and Eulerian approaches can be found in the literature.

3.1. Whole lung vs. local scale approach

In the whole lung approach, the lung is viewed as a system of branching tubes. Because of the enormous complexity of the airway system, airflow and transport and deposition of inhaled particles are de-coupled and hence are treated independently. Consequently, particle deposition in individual airways is only indirectly connected to the airflow pattern by using analytical deposition equations for pre-specified flow conditions, e.g. for laminar flow conditions, thus simulating the average behaviour of many particles.

In the local scale approach, only deposition in selected components of the human respiratory tract, e.g. nasal airways, bronchial airway bifurcations or alveolar ducts and sacs, is considered. However, this geometric limitation permits the correlated solution of air flow and particle transport equations by numerical methods, e.g. by finite elements. Such two- or three-dimensional fluid dynamics and particle trajectory models provide information on particle deposition patterns within structural elements of the lung, thus simulating the behaviour of individual particles.

3.2. Langrangian vs. Eulerian approach

In the Lagrangian approach, trajectories of single particles are tracked through the whole lung (whole lung models) or through single or multiple airway bifurcations (local scale models). For example, the random walk of individual inhaled particles through the stochastic lung model has been simulated by Monte Carlo methods (Koblinger & Hofmann, 1990; Hofmann & Koblinger, 1990, 1992). Particle trajectory simulations in airway bifurcations have been presented, among others, by Balásházy and Hofmann (1993a, 1993b), Balásházy (1994), Comer et al. (2001a, 2001b), Martonen et al. (1997), Zhang and Kleinstreuer (2002), and Zhang et al. (2002a, 2002b, 2008). These particle trajectory simulations have to be repeated many times, say a few ten thousand times, to obtain statistically significant average deposition efficiencies, deposition fractions, and particle deposition patterns.

In the Eulerian approach, a population of particles is tracked through the human airway system and deposition in a given airway generation is given by the difference between incoming and outgoing number or mass of particles or related particle or mass concentrations. Examples of the Eulerian approach at the whole lung level are the deterministic generation-based deposition models (Hofmann et al., 1989; Martonen, 1993; Yeh & Schum, 1980), the one-dimensional trumpet model (Egan & Nixon, 1985; Mitsakou et al., 2005; Taulbee & Yu, 1975), and the multiple path models (Anjilvel & Asgharian, 1995; Asgharian et al., 2001). As an example for local scale models, Gradon and Orlicki (1990) applied this approach to an airway bifurcation model.

4. Aerosol deposition models for the whole lung

Deposition calculations start with the determination of the inhalability of particles in ambient air, where inhalability is defined as the ratio of the number concentration of particles inspired through the nose or mouth to the number concentration of particles present in the ambient air volume. Depending on atmospheric conditions, i.e. still air or high windspeed, the inhalability drops from 1 at particle sizes of few micrometres, to about 0.5 for particles in the size range of 30–50 μm (ICRP, 1994).

At the onset of inhalation, particles pass through the extrathoracic region, bronchial and acinar airways and, after a short breath-hold time, follow the same path back during the exhalation phase. Their depth of penetration into the lungs depends on the time during the inhalation phase at which they are inhaled. For example, particles inhaled at the beginning of the inhalation phase may reach the peripheral acinar generations, while those inhaled at the end of the inspiration phase may already stop in the nose or mouth. In terms of deposition calculations, this particle transport scenario requires the computation of deposition efficiencies or fractions in extrathoracic, cylindrical bronchial and alveolated acinar airways for the whole breathing cycle.

In general, the two primary differences among currently available models of inhaled particle deposition in the whole lung are (i) the choice of the selected morphometric lung model, and (ii) the applied computational techniques generally related to the complexity of the selected morphometric model. In the following sections, the modelling philosophy of several particle transport and deposition models will be discussed and their strengths and limitations evaluated. Rather than to provide a comprehensive review of all deposition models ever published, five different classes of conceptual models will be discussed according to lung morphometry and mathematical modelling technique: (1) semi-empirical regional compartment models, (2) one-dimensional cross-section or "trumpet" models, (3) deterministic symmetric generation or "single path" models, (4) deterministic asymmetric generation or "multiple-path" models, and, (5) stochastic asymmetric generation or "multiple-path" models. Models 2 to 5 are often termed "mechanistic models" as they are based on a mechanistic understanding of physiological and physical mechanisms, while Model 1 is based primarily on mathematical fits to experimental data.

4.1. Semi-empirical regional compartment models

For radiological protection purposes, the International Commission on Radiological Protection (ICRP, 1994) has proposed a semi-empirical model for regional deposition in the human respiratory tract. The morphometric model consists of 4 anatomical regions (see Fig. 3): (1) the extrathoracic region (ET), comprised of the anterior nasal passages (ET_1) and the posterior nasal passages, the naso- oropharynx, and the larynx (ET_2); (2) the bronchial region BB, consisting of trachea and bronchi; (3) the bronchiolar region (bb), consisting of bronchioles and terminal bronchioles; and (4) the alveolar-interstitial region (AI), consisting of respiratory bronchioles and alveolar ducts and sacs surrounded by alveoli. Inhalability is treated as an additional region only during the inhalation phase. The definition of these compartments is strongly influenced by the specific clearance mechanisms associated with each compartment. For instance, deposition in the BB and bb regions is also termed the fast-cleared fraction of deposition, and deposition in the AI region is also termed the slow-cleared fraction (*note*: a slow clearance fraction in BB and bb airways have been observed in retention measurements by Stahlhofen (1989), Stahlhofen et al. (1995), and Smith et al. (2008).

For particle deposition calculations, the human respiratory tract is treated as a series of filters (regions) through which inhaled particles are passing during inspiration and back again during expiration. Each of these filters is defined by two characteristic parameters, the fraction of tidal air that reaches a given filter i, φ_i, and the deposition efficiency of that filter, η_i. Regional deposition efficiencies η_i for inhalation and exhalation are described by semi-empirical equations of the form:

$$\eta = 1 - \exp(-aR^p) \tag{1}$$

where a and p are constants and R is a function of particle size and flow rate (or related thermodynamic and aerodynamic parameters), which were derived from mathematical fits to available experimental data (Rudolf et al., 1986, 1990, 1994; Stahlhofen et al., 1989).

Deposition in different lung regions is commonly expressed by deposition fractions, which are defined as the fraction of inhaled particles reaching that region, multiplied by the deposition efficiency of that region. To illustrate the results obtained with the ICRP model, deposition fractions in ET_1, ET_2, BB, bb and AI are plotted in Fig. 4 for a male worker engaged in light work under nasal breathing conditions (ICRP, 1994).

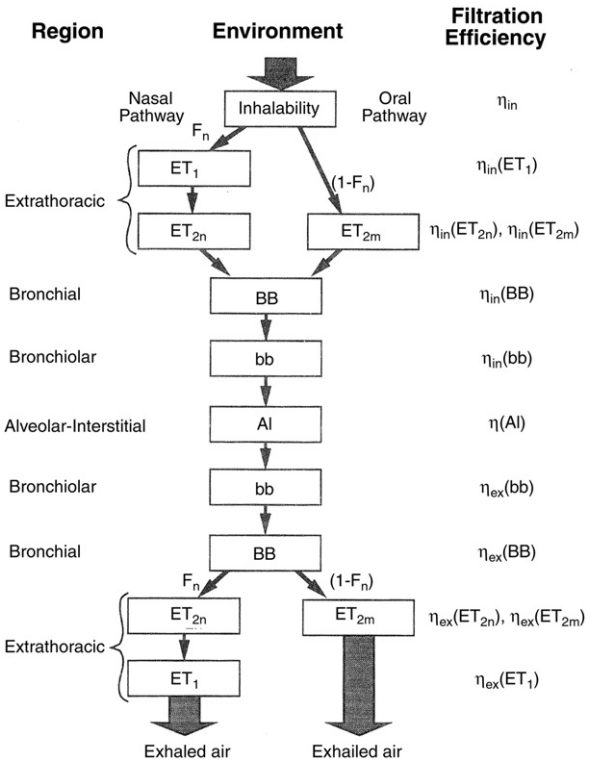

Fig. 3. Empirical representation of inhalability of particles and their deposition in the extrathoracic (ET), bronchial (BB), bronchiolar (bb), and alveolar-interstitial (AI) regions in the human respiratory tract during continuous breathing by transport through a series of filters (ICRP, 1994).

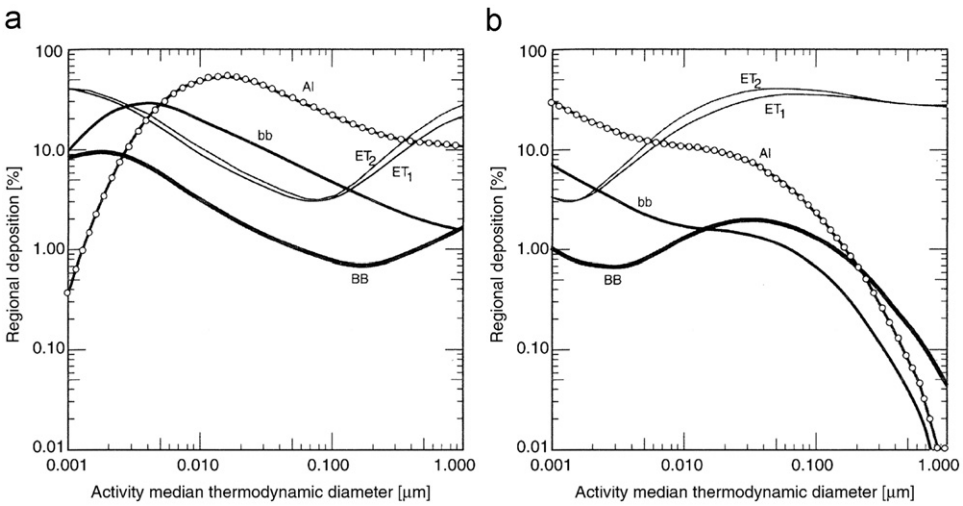

Fig. 4. Fractional deposition in each region of the human respiratory tract for a nose-breathing reference worker with an average breathing rate of 1.2 $m^3\ h^{-1}$, shown as a function of the activity median thermodynamic diameter, AMTD (panel A), and the activity median aerodynamic diameter, AMAD (panel B). Deposition is expressed as the fraction of the activity present in ambient air that is inspired (particle density = 3.0 g cm^{-3}, shape factor = 1.5) (ICRP, 1994).

The major benefit of such semi-empirical models is that they are based on actually measured data in human volunteers. The pre-fix "semi" refers to the fact that measured deposition fractions were analysed in terms of fluid and particle parameters to allow its application to all particle sizes and breathing patterns. However, there are two limitations to the experimental data: First, tracheobronchial (TB), i.e. BB and bb, and AI depositions are derived indirectly from retention measurements, where the fast-cleared fraction is identified as tracheobronchial deposition and the slow-cleared fraction

as AI deposition (*note*: the experimental observation of a slow bronchial clearance fraction was not yet considered for the interpretation of bronchial and acinar deposition). Secondly, since deposition in BB and bb cannot be separated experimentally, it has to be based on modelling assumptions, thus representing no longer true experimental data.

Another favourable feature of semi-empirical models is the relatively simple morphometric structure of the lung (only 4 regions), which does not require sophisticated computer programs, thereby facilitating the application of the ICRP model. Moreover, this computer code can be purchased readily by anyone interested in total and regional deposition calculations, which may explain its popularity among researchers who simply want to apply a model without more in-depth knowledge. On the downside, however, the greatly simplified morphometry of the ICRP model is also its major limitation, as it cannot, by definition, provide information about particle deposition within a given region, e.g. in single airway generations.

4.2. One-dimensional cross-section or "trumpet" models

In this model, the human airway system is approximated by a one-dimensional, variable cross-section channel, where the cross-sections are functions of the generation number of a given symmetric lung model, typically the Weibel (1963) model A (Taulbee & Yu, 1975). Thus each airway branch within a given generation has identical dimensions and is characterized by its axial distance from the origin of the trachea. In the acinar generations, additional volume for the alveoli encircles the channel. The cross-sectional area increases sharply with distance from the trachea adopting a trumpet-like shape, hence the name "trumpet" model (Fig. 5).

The breathing process is pictured as the movement of air into and out of this channel as airway and alveolar volumes expand and contract uniformly. The airflow velocity and the particle concentration (Eulerian approach) at a given depth in the model are considered to be the averages over all airways in the corresponding generation. The transport of inhaled particles by convection and axial diffusion, their deposition along the channel, and mixing between tidal air and reserve volume are described mathematically by a mass balance equation with different loss terms for the various deposition mechanisms, using analytical equations for deposition by diffusion, sedimentation and impaction. The transport equation can be solved either analytically (without axial diffusion) or by numerical methods for more complex initial and boundary conditions.

Initially developed by Taulbee and Yu (1975), and subsequently modified by Taulbee et al. (1978), the trumpet model was further developed by Egan and Nixon (1985), Nixon and Egan (1987), and Darquenne and Paiva (1994), using more recent deposition equations. Recently, this model was extended by Lazaridis et al. (2001), Robinson and Yu (2001), Mitsakou et al. (2005), and Choi and Kim (2007) by incorporating dynamic processes affecting the size of the inhaled aerosol, such as hygroscopic growth, coagulation, electrical charge, and gas phase chemical reactions.

The transport and deposition of particles due to the simultaneous action of different processes was described by Mitsakou et al. (2005) by a time-dependent differential equation for the cross-sectional area A_T of all airways and alveoli at distance x and particle number concentration N_i in the particle size bin i in an one-dimensional channel with airway length (or equivalent airway generation number) x:

$$\partial t(A_T N_i) = -\partial/\partial x(A_A u N_i) + \partial/\partial x(A_T D_{effi} \partial N \partial_i / x) - V_{di} n \pi d_T N_i + (\partial/\partial t(A_T N_i)_{growth} + \partial/\partial t(A_T N_i)_{coagulation}. \quad (2)$$

If d_T is the diameter of an individual airway at distance x from the trachea, then the cumulative cross-sectional area $A_T = n\pi d_T^2/4$, where n is the total number of airways corresponding to x. A_A represents the cumulative cross-sectional area of the airways where convective transport occurs at distance x, i.e. without the alveolar volume, u the air velocity, D_{effi} the effective axial diffusion coefficient, and V_{di} the deposition velocities due to gravitational settling, inertial impaction, and Brownian motion.

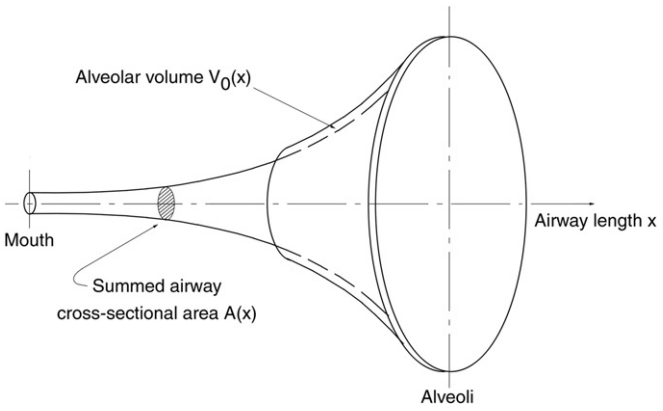

Fig. 5. Illustration of the one-dimensional, variable cross-section or "trumpet" model (Taulbee & Yu, 1975).

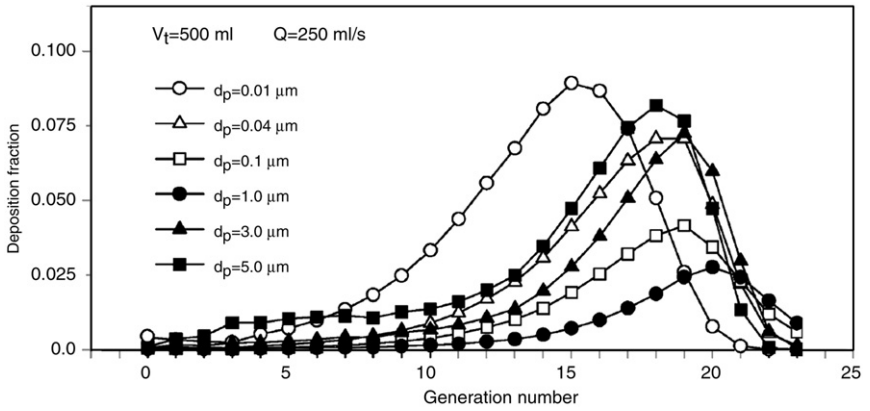

Fig. 6. Generational deposition fractions predicted by the trumpet model of Choi and Kim (2007) for particle diameters ranging from 10 nm to 5 μm. Breathing parameters are: V_T=500 ml, Q=250 ml s^{-1}.

Diameters and lengths in Choi and Kim (2007) are also based on Weibel's (1963) model A. Deposition fractions produced by the dynamic one-dimensional cross-section model of Choi and Kim (2007) are presented in Fig. 6 for a wide range of particle sizes under defined breathing conditions (V_T=500 ml, f=15 min^{-1}), illustrating the diameter dependence of deposition fractions among thoracic airways.

A significant limitation of this approach is the rather crude airway geometry, which refers to generational airway volumes without internal airway structure. Consequently, trumpet models cannot simulate asymmetric effects of airway geometry and related flow rates. On the other hand, a positive feature of such models is the exact mathematical formulation and solution of differential equations describing transport and deposition phenomena, and the computationally convenient way to include several simultaneously acting mechanisms by simply adding specific loss terms to the right-hand side of Eq. (2).

4.3. *Deterministic symmetric generation or "single-path" (typical-path) models*

In the commonly used symmetric lung models (e.g. Weibel, 1963; Yeh & Schum, 1980; James, 1988), all airways in a given airway generation have identical linear dimensions, and each parent airway branches into two identical daughter airways. Thus all pathways of an inhaled particle from the trachea to the alveolar sacs are identical and thus can be represented by a single path. This is illustrated in Table 1 for the typical path lung model of Yeh and Schum (1980). Because of the symmetric branching, the inhaled airflow and entrained inhaled particles are equally distributed among all airways in a given generation, leading to identical deposition fractions in each airway. Deposition efficiencies are computed by applying analytical deposition equations for specified flow conditions in straight cylindrical tubes for the different physical deposition mechanisms (see Table 2). Deposition fractions in a given airway generation are then obtained by multiplying the corresponding deposition efficiencies by the fraction of particles (number or mass concentration) reaching that airway generation (Eulerian approach).

Current deterministic, symmetric deposition models differ primarily by the implementation of different morphometric lung models and analytical deposition equations (see sections on morphometric lung models and physical deposition mechanisms). Starting with the first whole lung deposition model by Findeisen (1935), subsequent developments by Landahl (1950), Altshuler (1959), Beeckmans (1965), Gerrity et al. (1979), Hofmann (1982a), Hofmann et al. (1989), Martonen (1982, 1983, 1993), Martonen et al. (1989), and Yeh and Schum (1980), among others, reflect the ever increasing availability of more detailed morphometric information on lung structure and airway dimensions and more realistic analytical deposition equations. The Yeh and Schum (1980) deposition model also forms the morphometric and physical basis of the US National Commission on Radiological Protection (NCRP) respiratory tract model (National Commission of Radiological Protection (NCRP), (1997); Phalen et al., 1991). Further model developments refer to the application to specific lung morphologies (e.g. children, lung diseases), or to the inhalation of radioactive aerosols, without any major changes of the modelling philosophy.

Deposition fractions for particle diameters ranging from 10 nm to 10 μm are plotted in Fig. 7 for sitting breathing conditions (ICRP, 1994), using the DEPOS code (Hofmann, 1982a), which is based on the Yeh and Schum (1980) model. To facilitate comparison between different morphometric lung models, all computed generational deposition fractions presented in this paper start with generation 0 for the trachea. Computed deposition fractions are normalized to the number of particles entering the trachea, i.e. extrathoracic deposition has been excluded. Such normalization does not affect the relative distribution of inhaled particles within the thoracic region of the human respiratory tract as deposition fractions in all airway generations are reduced by the same fraction (1–*ET* deposition). The diameter dependence of the deposition patterns resembles the results presented in Fig. 6 for the trumpet model of Choi and Kim (2007).

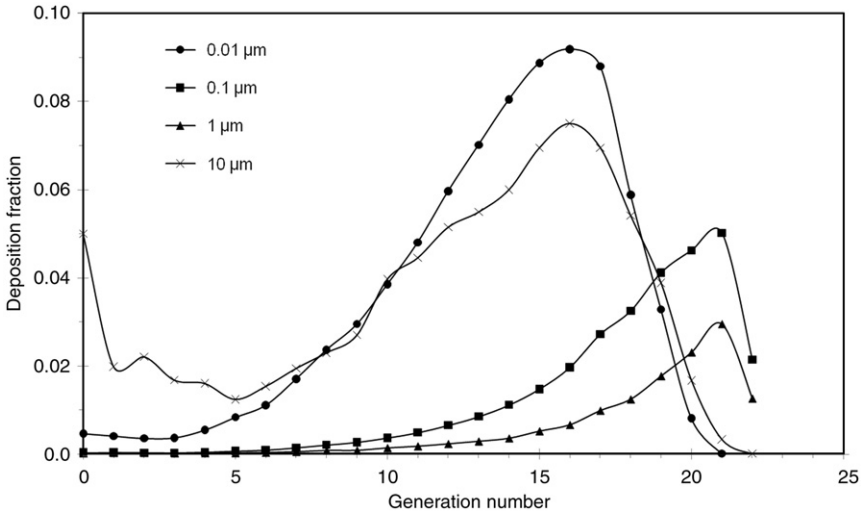

Fig. 7. Deposition fractions predicted by the deterministic symmetric generation model DEPOS for a wide range of particle diameters and nasal sitting breathing conditions.

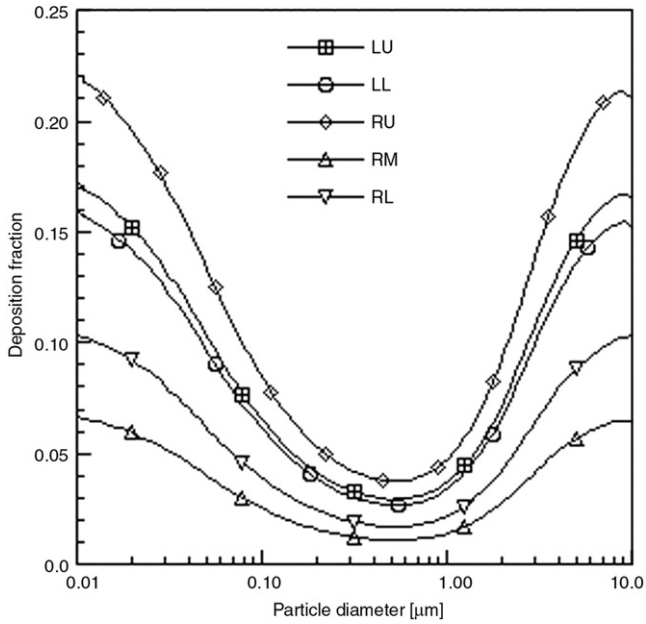

Fig. 8. MPPD model predictions of lobar deposition for resting breathing conditions. LU: left upper lobe, LL: left lower lobe, RU: right upper lobe, RM: right middle lobe, RL: right lower lobe (Asgharian et al., 2001).

The major practical advantage of such single-path models is their geometric simplicity because a single average path does not require detailed knowledge of the branching structure and the ventilation of the lung. From a modelling point of view, these models are not computationally demanding and have therefore been used frequently. Conversely, this morphometric simplicity and inherent relationship between deposition equations for different physical mechanisms and related fluid dynamics limits the application of such models for the prediction of realistic deposition patterns in asymmetric and variable lung structures.

4.4. Deterministic asymmetric generation or "multiple-path" models

Multiple-path models are more realistic than single-path models because they are based on actual measurements of single airways and their branching structure rather than on average values, and thus reflect the asymmetric branching

pattern of the lung. However, a complete deterministic asymmetric description of the human lung is presently not available. The first step towards introducing lobar asymmetry was the 5-lobe lung model of Yeh and Schum (1980), although single-path descriptions were assumed for each lobe. In the multiple-path particle deposition (MPPD) model of Asgharian et al. (2001), the bronchial airway geometry is represented by 50 structurally different multiple-path models derived from the stochastic lung model (Asgharian et al., 2001; Hofmann et al., 2002), assuming the same probability density functions and parameter correlations as those found in the lung casts measured by Raabe et al. (1976) and statistically analysed by Koblinger and Hofmann (1985). These bronchial trees were either supplemented by attaching identical acini to each terminal bronchiole based on the typical-path model of Yeh and Schum (1980) or by a stochastic acinar model, which considers the additional variability in the number of acinar pathways and linear dimensions (Koblinger & Hofmann, 1990). Since deposition in the acinar region by diffusion and sedimentation is driven by volume rather than by structure, the structural organization of the acinar region hardly affects resulting deposition fractions. Thus the MPPD model considers the branching asymmetry of airways and related flow rates, and thus allows the calculation of lobar deposition, which cannot be predicted by symmetric lung models.

At an airway bifurcation, the airflow in each asymmetrically branching airway is assumed to be proportional to its distal volume, and computed by a procedure known as "tree traversal" (Anjilvel & Asgharian, 1995). For each airway of the lung, particle concentrations as a function of time were determined for the proximal and distal ends (Eulerian approach). Knowing the concentration of particles at the proximal end of an airway, the concentration at its distal end was calculated by considering the deposition efficiencies for the various deposition mechanisms.

Calculated deposition fractions in the 5 lung lobes, having different volumes and consequently different airway dimensions and number of airway generations, are illustrated in Fig. 8 for resting breathing conditions (Asgharian et al., 2001). The notable differences of deposition fractions among the individual lobes indicate that particle deposition, and thus resulting health effects, within the lung is highly non-uniform.

The main advantage of such multiple-path models over the commonly used symmetric models are: (1) exact solutions of the mass balance equations can be obtained in a realistic, i.e. asymmetric, lung structure; (2) the determination of average deposition fractions is based on a more realistic description of the human airway morphology; and, (3) the asymmetry of the lung geometry allows the determination of intra- and inter-subject variations in airway generations or lung regions, and between lobes. Their primary limitation at this moment is that morphometric data are presently only available for large bronchial airways and, moreover, only for a single lung, so that the measured airway morphometry has to be supplemented by structurally different deterministic multiple-path models derived from the stochastic lung models described in the following section.

4.5. *Stochastic asymmetric generation or "stochastic multiple-path" models*

A fully stochastic deposition model, simulating the trajectories of single particles (Lagrangian approach) was originally presented by Koblinger and Hofmann (1990), and Hofmann and Koblinger (1990, 1992) and further developed by Hofmann and Bergmann (1998) and Hofmann et al. (2002). This deposition model is continuously revised when new data become available or additional mechanisms are implemented, such as particle clearance (Hofmann & Sturm, 2004). The currently used stochastic airway geometry is based on rigorous statistical analyses of the morphometric data of bronchial (Raabe et al., 1976) and acinar (Haefeli-Bleuer & Weibel, 1988) airways (Koblinger & Hofmann, 1985, 1990).

In the stochastically asymmetric deposition model IDEAL (Inhalation, Deposition and Exhalation of Aerosols in the Lung) of Koblinger and Hofmann (1990) and Hofmann and Koblinger (1990, 1992), the term "stochastic particle deposition" refers to the transport of inspired particles through a stochastic asymmetric lung structure by randomly selecting a sequence of airways for each individual particle, and to the application of stochastic modelling techniques, in this case the Monte Carlo method. The branching airway system is modelled by a sequence of Y-shaped airway bifurcation units consisting of a parent tube and two randomly and asymmetrically dividing daughter airways. The philosophy to describe the lung geometry by bifurcations instead of cylindrical airways was the then expectation to implement results of CFPD calculations into the deposition model once they become available (e.g. Balásházy, 1994; Farkas & Balásházy, 2008; Hofmann et al., 2001; Zhang et al., 2001). The use of airway bifurcation numbers instead of airway generation numbers is, however, a mere question of bookkeeping and does not affect particle deposition calculations (*note*: deposition in bifurcations can easily be converted to deposition in straight cylindrical airways). For the simulation of random paths through the lungs, the geometric properties of the two daughter airways are randomly selected at each bifurcation from their probability density functions, although constrained by correlations among some of the parameters. The actual path of the particle through either the major or the minor daughter branch is randomly selected from the flow splitting distribution based on distal lung volumes. As a consequence of the variability of the selected sequence of airways, all paths of inspired particles are different from each other, and so are the deposition fractions in the individual airways. By simulating the random paths of many particles, typically of the order of tens or hundreds of thousands, statistical means can be calculated for total, regional and generational deposition, providing also information on the underlying statistical distributions.

Since information on transport and deposition of individual particles within airway bifurcations is limited at present to only a few selected bifurcation models, deposition in individual airways is currently based on the average behaviour of an ensemble of particles as given by analytical equations for different deposition mechanisms. To improve the statistics of the

Monte Carlo calculations by reducing the number of iterations, deposition of an inhaled particle is simulated by decreasing its statistical weight, i.e. the particle continues its path with a smaller statistical weight instead of starting again at the entrance into the lungs.

Deposition fractions among bronchial and acinar airway generations are plotted in Fig. 9 for 200 nm particles under sitting breathing conditions (ICRP, 1994), demonstrating the inherent asymmetry and variability of the human lung, such as the gradual transition from bronchial to acinar airways in airway generations 11–19 (panel A), and the variability of deposition fractions within a given airway generation (panel B), which can reasonably be approximated by lognormal distributions.

The main beneficial feature of a stochastic deposition model is the application of the most realistic lung structure presently available in terms of dimensional variability and branching asymmetry, which allows the calculation and quantification of the distributions of deposition fractions due to intra- and inter-subject variability, rather than only related average values. Moreover, deposition in individual subjects, which are different from those measured by Raabe et al. (1976), can be predicted by applying linear scaling factors, derived from pulmonary function tests, to linear airway dimensions, and/or by varying the statistical correlations among different parameters. Nevertheless, one must bear in mind that the stochastic lung geometry was derived from measurements of a single lung (partly supplemented by data

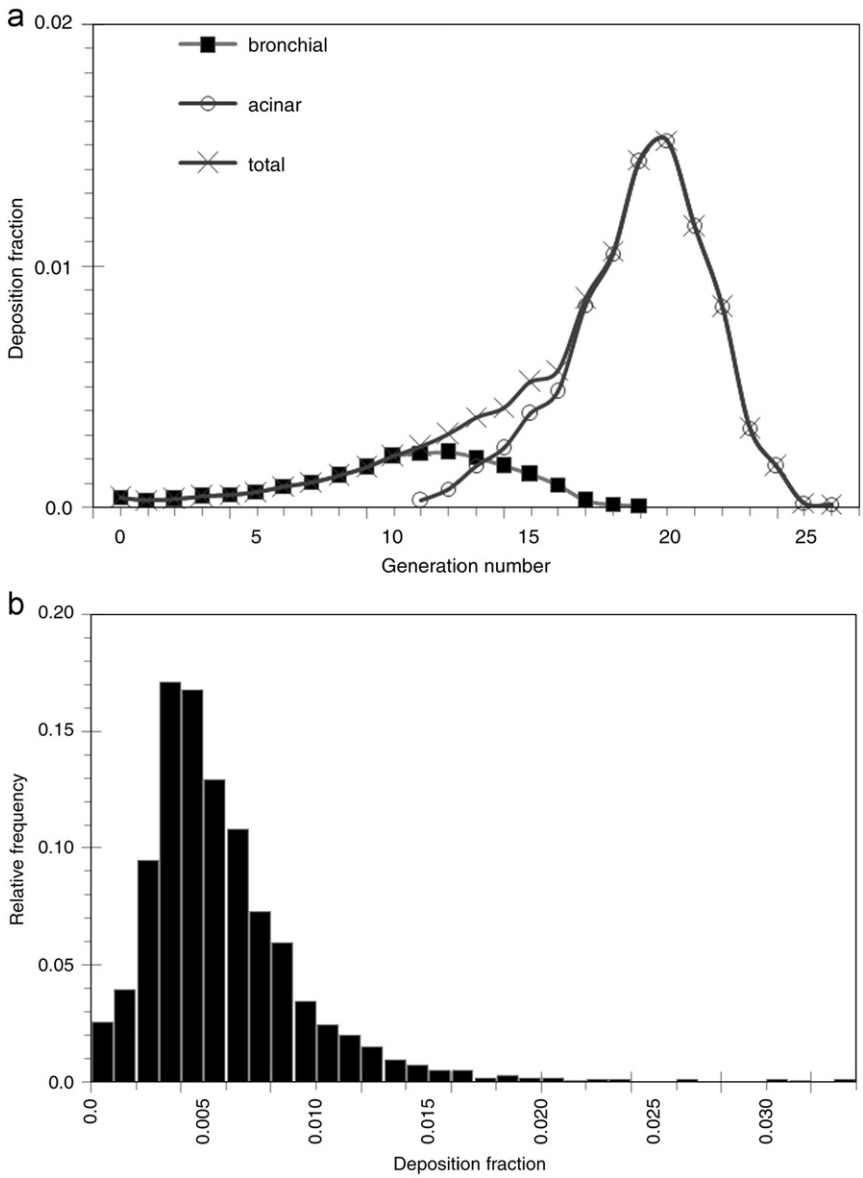

Fig. 9. IDEAL model predictions of deposition by generation (panel A) and variability within bronchial generation 15 (panel B) for 200 nm particles and nasal sitting breathing conditions (ICRP, 1994) (Hofmann et al., 2002).

from a second lung) and hence may not be representative for a specific individual. However, this limitation applies to all currently available morphometric lung models.

5. Which deposition quantities can be predicted by current models?

Health effects in human lungs following inhalation of airborne particles are commonly related to deposition fractions for the whole lung or a given lung region or a given group of airway generations during a single breath. Such deposition patterns are normalized either to the number of particles entering the trachea, if only the relative distribution within the lungs is required, or to the number of particles entering the nose or the mouth by considering pre-filtration by nasal or oral passages, if the absolute values and/or the distribution within the whole respiratory tract is needed. While the first normalization demonstrates the exclusive effect of lung geometry on deposition in the lungs, the second normalization represents the real inhalation situation (*note*: for high extrathoracic deposition efficiencies, only a few particles will enter the lung).

Deposition fractions are commonly related to the number of particles inhaled during a single breath. For continuous exposures, cumulative deposition fractions per unit time, e.g. minutes or hours, may be more appropriate indicators of risk. Such cumulative deposition fractions can be obtained by multiplying the deposition fractions per single breath with the number of breaths per minute or hour.

Current deposition models can predict the following deposition quantities relevant for the assessment of health effects in the lungs: (1) total deposition; (2) regional deposition; (3) generational deposition; and (4) lobar deposition. For each deposition quantity, the results obtained by the five conceptual models discussed in the preceding chapter will be compared to examine the role of lung morphometry and mathematical modelling technique used in each of these models. Unfortunately, deposition fractions published by the various authors were calculated for a variety of particle parameters and breathing patterns, which makes a model comparison difficult to interpret. Thus to enable a reasonable comparison, some of these authors (Marsh, J.W., Kim, C.S., Robinson, R.J., & Asgharian, B.), representing all five classes of deposition models, volunteered to provide new deposition data for the same set of particle properties and breathing parameters. To further facilitate comparison between the different models, each morphometric lung model was normalized to an FRC of 3300 ml.

5.1. Total deposition

To investigate potential similarities and differences among the different models, theoretical predictions of total deposition of unit density particles as a function of particle size, ranging from 1 nm to 10 μm, are plotted in Fig. 10 for nasal inhalation under sitting breathing conditions (V_T=750 ml, f=12 min^{-1}) (ICRP, 1994). While all models predict the same U-shaped dependence of total deposition on particle diameter, some differences in the absolute values can be observed. In general, all deposition fractions lie within a range of about ± 10%. These differences are presumably caused by the application of different morphometric lung models, analytical deposition equations and modelling techniques.

The typical U-shape of the total deposition curve is caused by the dominance of Brownian motion for particles below about 0.1 μm and of inertial impaction and gravitational settling above about 1 μm. Corresponding calculations for oral inhalation reveal similar deposition patterns. While nasal and oral inhalations exhibit practically the same total deposition

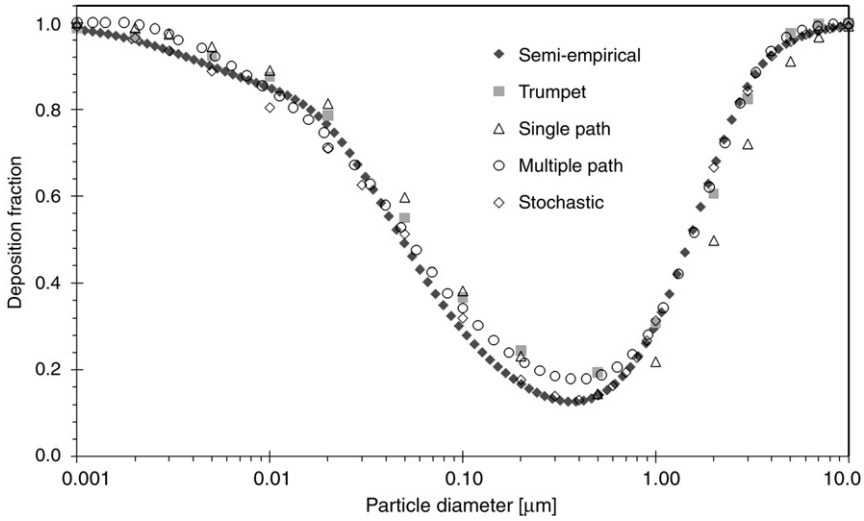

Fig. 10. Comparison of model predictions of total deposition for unit density particles ranging from 1 nm to 10 μm under nasal sitting breathing conditions (ICRP, 1994), applying 5 different deposition models: semi-empirical (ICRP, 1994), trumpet (Choi & Kim, 2007), single path (Hofmann, 1982a), multiple path (Asgharian et al., 2001), and stochastic (Koblinger & Hofmann, 1990).

for small particles, the nose is for large particles a more effective filter than the mouth. Similarity among the different models was also found for flow rates characteristic of resting, and light and heavy physical activities (ICRP, 1994), reflecting the dependence of diffusional, inertial and gravitational deposition mechanisms on flow rate.

5.2. Regional deposition

For extrathoracic deposition, a variety of semi-empirical equations are currently used in the different deposition models for inhalation and exhalation, for nasal and oral inhalation, and for small and large particles. Semi-empirical equations were derived either from measurements in human subjects or in nasal and oral casts (e.g. Cheng, 2003; Cheng et al., 1996; Kesavanathan & Swift, 1998; Stahlhofen et al., 1989; ICRP, 1994; NCRP, 1997; Subramaniam et al., 2003). For example, nasal depositions predicted by the different models are shown in Fig. 11 for sitting breathing conditions (ICRP, 1994), illustrating the effect of different semi-empirical formulations on nasal deposition. As for total deposition, nasal deposition also exhibits a U-shape. Indeed the U-shape of nasal deposition also contributes to the observed U-shape for total deposition. While all models predict the same dependence on particle diameter, some variations of the absolute values can be observed. Except for nanometre-sized particles, all deposition fractions lie within a range of about $\pm$ 10%.

Deposition fractions for the trachebronchial region predicted by the different deposition models are plotted in Fig. 12A for sitting physical activity (ICRP, 1994) and nasal inhalation (ICRP, 1994). Deposition fractions in the TB region form a saddle-shaped curve with two peaks. Below the nano-sized peak and above the micron-sized peak, deposition fractions drop rapidly to smaller deposition fractions due to the high filtering efficiency of small and large particles in the nasal passages (see Fig. 11), which reduces inspiratory thoracic depositions of these particle sizes. Corresponding deposition fractions for the acinar region are shown in Fig. 12B. Again, deposition in the acinar region exhibits a saddle-shaped curve with two peaks. The apparent reduction of deposition fractions at very small, say below about 3 nm, and relatively high, say above about 5 μm, particle diameters is caused not only by high extrathoracic deposition efficiencies, but also by the upstream TB deposition efficiencies for these particle sizes. Despite these variations of nasal filtration in the various deposition models, they all exhibit the same functional relationship with particle diameter.

5.3. Generational deposition

Distributions of deposition fractions of 20 nm unit density particles among bronchial and acinar airway generations are illustrated in Fig. 13 for sitting breathing conditions (ICRP, 1994) and nasal inhalation. The shapes of the distributions indicate that most of the inhaled particles are deposited in the peripheral acinar airways. Although deposition efficiencies increase upon penetration into the lung, the number of particles actually reaching these airways dramatically drops due to the filtration effect in preceding airways. While all four deposition models predict the same shape of the deposition curve, differences in peripheral airways can be observed, consistent with acinar deposition fractions displayed in Fig. 12 (*note*: the semi-empirical ICRP (1994) model does not allow the prediction of generational deposition fractions).

The preferential deposition in peripheral acinar airways suggests that resulting health effects may occur primarily in that anatomical region. However, such an approach does not consider the surface areas of airway generations onto which these particles are deposited. Deposition densities (or "local doses") in a given airway generation can be obtained by

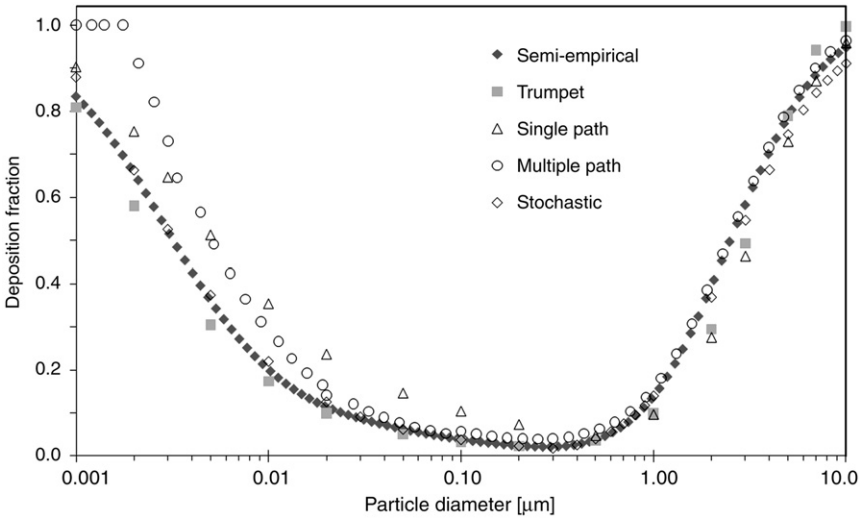

Fig. 11. Comparison of model predictions of nasal deposition for unit density particles ranging from 1 nm to 10 μm under nasal sitting breathing conditions (ICRP, 1994), applying 5 different deposition models: semi-empirical (ICRP, 1994), trumpet (Choi & Kim, 2007), single path (Hofmann, 1982a), multiple path (Asgharian et al., 2001), and stochastic (Koblinger & Hofmann, 1990).

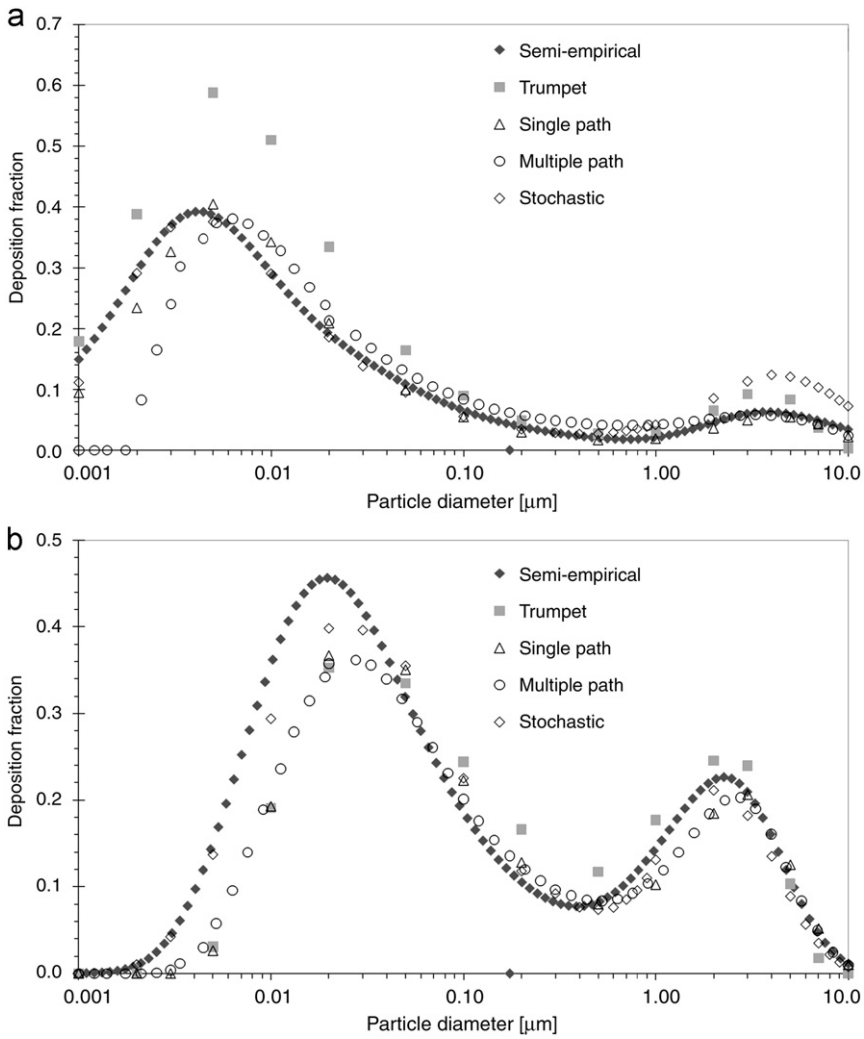

Fig. 12. Comparison of model predictions of bronchial (panel A) and acinar (panel B) deposition for unit density particles ranging from 1 nm to 10 μm under nasal sitting breathing conditions (ICRP, 1994), applying 5 different deposition models: semi-empirical (ICRP, 1994), trumpet (Choi & Kim, 2007), single path (Hofmann, 1982a), multiple path (Asgharian et al., 2001), and stochastic (Koblinger & Hofmann, 1990).

dividing the deposition fraction in a given generation by the surface area of that airway and by the total number of bronchial airways in that generation (Hofmann et al., 2006). Since the higher deposition fractions in peripheral bronchiolar and acinar airways are more than compensated by their larger surface areas, related deposition densities continuously decrease in the deeper lung. The resulting distribution of deposition densities is then more compatible with the histologically observed distribution of bronchial carcinomas, which were preferentially found in upper and central bronchial airways (Veeze, 1986).

5.4. Lobar deposition

Lung diseases caused by the inhalation of particulate matter have often been reported to occur at specific sites in the lung, particularly within specific lobes (Parkash, 1977; Igarashi et al., 1987; Pityn et al., 1995). For example, Parkash (1977) found that lung carcinomas are more likely to develop in the right than in the left lung, and more likely in the upper than in the lower lobes. He further postulated that this site specificity ought to correlate more with the localized deposition pattern than with biological factors.

Fractional deposition data among the five lung lobes, reported by Asgharian et al. (2001), were already shown in Fig. 8, exhibiting significant differences among the individual lobes. Consistent with the U-shaped total deposition curve, the dependence of lobar deposition on particle diameter follows the same pattern. Corresponding generational deposition patterns within each lobe, generated by the stochastic lung model, are illustrated in Fig. 14 for 2 μm-sized particles under oral sitting breathing conditions (Winkler-Heil & Hofmann, 2009). While lobar deposition fractions differ among the

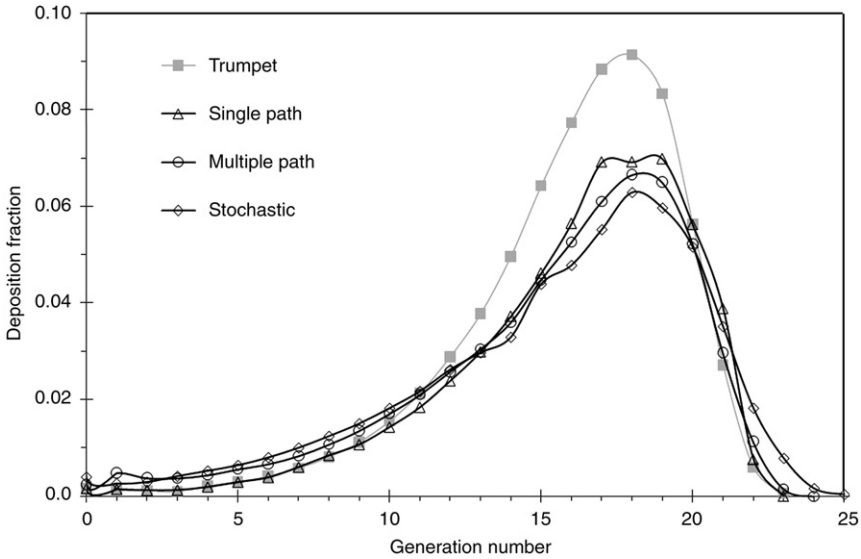

Fig. 13. Comparison of model predictions of deposition fractions among human airway generations under sitting breathing conditions (ICRP, 1994) for 20 nm unit density particles, normalized to the number of particles entering the trachea, applying 4 different deposition models: trumpet (Choi & Kim, 2007), single path (Hofmann, 1982a), multiple path (Asgharian et al., 2001), and stochastic (Koblinger & Hofmann, 1990). In airway generations 11–20, the deposition fractions predicted by the multiple path and stochastic models represent the sum of deposition fractions in bronchial and acinar airways.

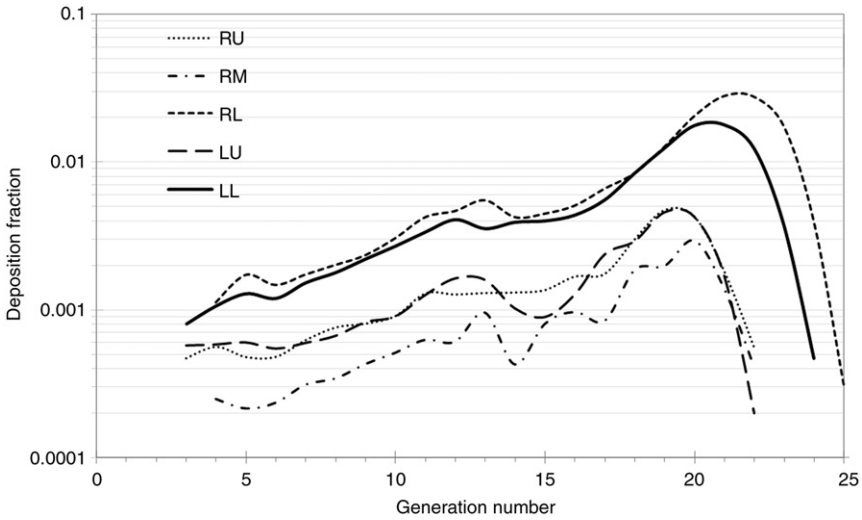

Fig. 14. Lobar deposition densities of 2 μm unit density particles predicted by the stochastic deposition model IDEAL for oral sitting breathing conditions (ICRP, 1994). LU: left upper lobe, LL: left lower lobe, RU: right upper lobe, RM: right middle lobe, RL: right lower lobe.

various lobes, their relative distribution among the airways of a given lobe is practically the same in all lobes. Differences in pathlengths within each lobe are caused by differences in corresponding lobar volumes. Similar results were reported by Subramaniam et al. (2003), based on the MPPD model (Asgharian et al., 2001) (*note*: only the MPPD and IDEAL models can predict lobar deposition as they are based on an asymmetric lung geometry). By dividing lobar (Fig. 8) or lobar generational deposition fractions (Fig. 14) by the corresponding surface areas provides information about related deposition densities or "doses" (Winkler-Heil & Hofmann, 2009).

5.5. Capabilities and limitations of whole lung models

Whole lung generation models permit the prediction of particle deposition in single airways or airway generations in currently available morphometric lung models for any combination of particle size and breathing pattern, except for the semi-empirical models which are restricted to regions accessible to measurements. By integration over a defined sequence of airway generations, average generational, lobar, regional or total deposition can be obtained.

The major differences between the modelling predictions produced by the different deposition models are: (1) mechanistic models permit the prediction of deposition in single airway generations and lobes, while semi-empirical models allow only the calculation of total and regional deposition fractions; (2) only asymmetric morphometric lung models can calculate deposition in different lobes, and (3) deposition calculations using different deposition equations in a given lung model or different morphometric lung models with the same deposition equations indicate that deposition fractions are affected by the selection of a specific lung model and a specific set of deposition equations, although all models predict the same trends as functions of particle diameter and breathing parameters.

Despite the documented success of the deposition models described above, the following basic limitations of the whole lung approach must be recognized: (1) models cannot be validated by comparison with experimental in-vivo data at the single airway or airway generation level, only for total and regional deposition; (2) models cannot predict deposition in a specific human subject, only for the lung geometries represented by the various morphometric lung models; (3) models cannot provide information on deposition patterns within airways or airway bifurcations; and (4) models cannot consider geometric deviations from the assumed cylindrical shape of airways, such as bifurcations. The latter two require the application of "local scale models" based on CFPD methods.

6. Comparison of model predictions with experimental data

The previous section dealt with the capability of models to predict deposition quantities relevant for the assessment of health effects. The relevance of these predictions must be validated by comparison with the available experimental evidence, otherwise modelling would remain a purely intellectual, albeit fascinating exercise. However, not all deposition quantities that currently can be predicted by deposition models are verifiable by experimental methods. At present, the following experimental data can be used for model validation: (1) total deposition; (2) regional deposition; (3) local deposition in a group of successive airway generations; and (4) deposition in physical airway models and lung casts.

6.1. Total deposition

Total deposition data of monodisperse ultrafine and micrometre-sized particles have been reported by a number of authors, e.g. by Brand et al. (2000), Heyder et al. (1975, 1986), Hiller et al. (1962), Kim and Jaques (2004), Melandri et al. (1983), and Tu and Knutson (1984). Total deposition as a function of particle diameter can be studied by varying the route of inhalation, i.e. nasal or oral inhalation and flow rate, i.e. different breathing conditions. Theoretical predictions of total deposition of unit density particles as a function of particle size, computed by the stochastic deposition model IDEAL, are plotted in Fig. 12 for the nasal and oral inhalation route for defined breathing conditions (V_T=1000 ml, f=15 min^{-1}) and compared with the extensive set of experimental data provided by Heyder et al. (1986). The excellent agreement between stochastic IDEAL model predictions and the experimental data, demonstrated in Fig. 15, supports the validity of that model. The range of total deposition fractions predicted by other models relative to the experimental data is illustrated in Fig. 10 for nasal breathing conditions (*note*: if these data were also included, Fig. 10 would become too crowded).

Another test of the validity of model predictions is the dependence of total deposition on a wide range of breathing conditions. For example, model predictions by the stochastic lung model were compared with the experimental data of Heyder et al. (1986) and Schiller et al. (1988), indicating excellent agreement (Hofmann et al., 2003).

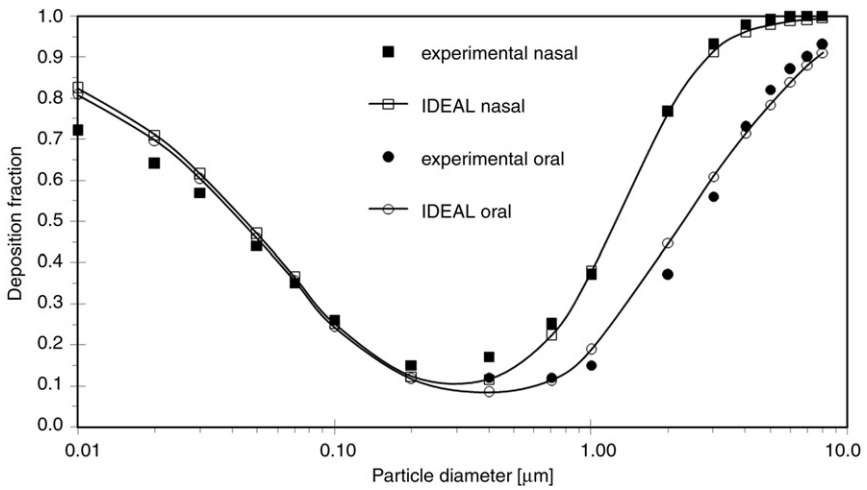

Fig. 15. Comparison of total deposition predicted by the stochastic deposition model IDEAL with the experimental data of Heyder et al. (1986) for a wide range of particle diameters under specified nasal and oral breathing conditions (V_T=1000 ml, f=15 min^{-1}).

In summary, the agreement between theory and experiment indicates that deposition models correctly predict total deposition within a relatively narrow range. It is important to emphasize here again that total deposition is the only deposition quantity, which can directly be measured in human subjects. Nevertheless, despite the many studies available, total deposition is only of limited use for the verification or falsification of specific deposition models and their parameters, as different generational or regional deposition fractions may fortuitously produce the same total deposition.

6.2. Regional deposition

Regarding regional deposition, i.e. deposition in extrathoracic, bronchial, and acinar regions, only deposition in the ET region can directly be measured in human subjects (see compilations of experimental data in ICRP (1994) and NCRP (1997). Some of these measurements in human subjects or in nasal and oral casts have been used to obtain semi-empirical nasal and oral deposition equations (e.g. Cheng et al., 1996; Cheng, 2003) and thus represent already experimental data. The effect of different semi-empirical deposition equations used in the various deposition models are illustrated in Fig. 11 for nasal breathing conditions. The significant variability of the deposition data found in the different studies, which may be attributed to intersubject variations (Cheng et al., 1996), raises, however, the question to what extent average ET deposition efficiencies are applicable to a specific person.

Tracheobronchial and acinar deposition cannot be measured directly, but can be derived from the analysis of retention measurements, which exhibit two distinct clearance phases: the fast-cleared fraction is assumed to represent TB deposition and the slow-cleared fraction deposition in the acinar region.

An alternative method to determine bronchial and acinar deposition experimentally is the application of the serial bolus technique (Kim & Hu, 1998; Kim & Jaques, 2000), where regional deposition is related to volumetric depths based on

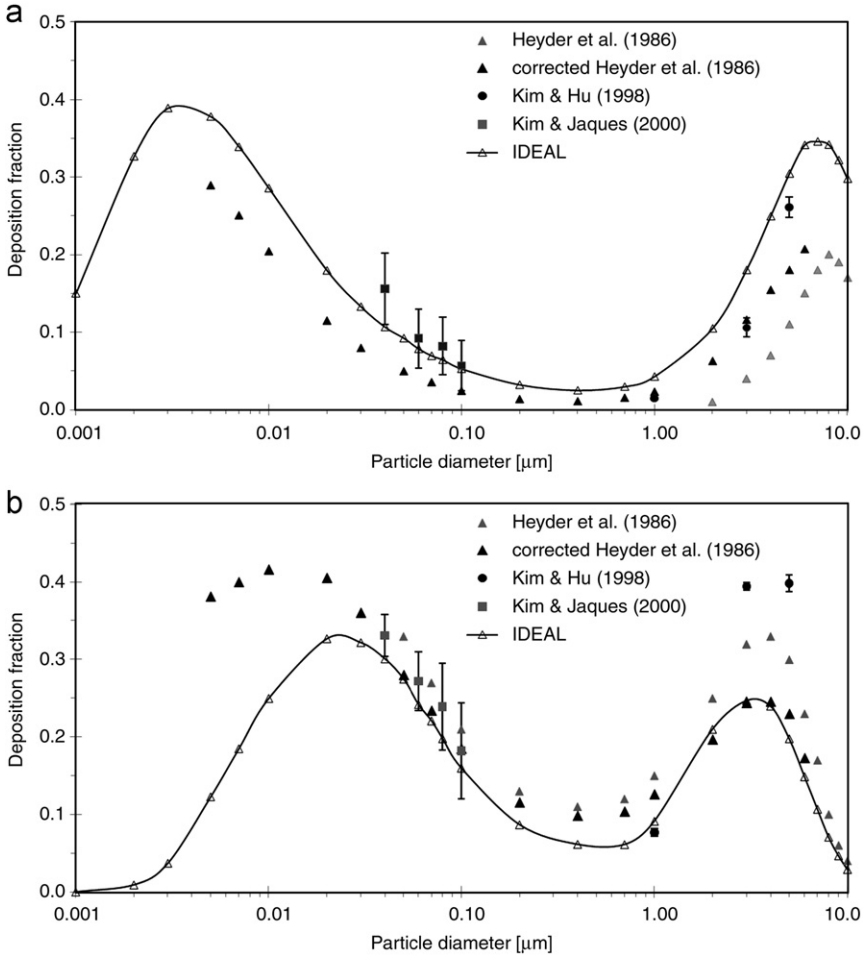

Fig. 16. Comparison of tracheobronchial (panel A) and acinar (panel B) deposition predicted by the stochastic deposition model IDEAL with experimental data (Heyder et al., 1986; Kim & Hu, 1998; Kim & Jaques, 2000) for specified oral breathing conditions (V_T=1000 ml, f=15 min^{-1}). The corrected data points of the Heyder et al. (1986) study refer to differences in oral deposition between modelling and experimental results, and to the effect of the slow bronchial clearance fraction on the identification of TB and A deposition (see related text).

Weibel's (1963) symmetric model A. Since the distinction between bronchial and acinar deposition is based on the cumulative volume incurred before and after generation 16 (terminal bronchioles), regional deposition is based on lung morphometry and not on clearance. However, these regional deposition data hinge upon the application of a specific lung model and thus represent only semi-experimental data.

Regional deposition in tracheobronchial and acinar regions has been measured in the past by several authors, e.g. Chan and Lippmann (1980), Foord et al. (1978), Heyder et al. (1986), Stahlhofen et al. (1980), Kim and Hu (1998), Kim and Jaques (2000), and Stahlhofen et al. (1989). Bronchial and acinar deposition fractions predicted by the IDEAL model for oral inhalation are compared in Fig. 16A (bronchial) and B (acinar) with the experimental data of Heyder et al. (1986), covering a wide range of particle sizes from 5 nm to 15 μm, of Kim and Hu (1998) for micron-sized particles, and of Kim and Jaques (2000) for ultrafine particles, which were inhaled through a mouthpiece. While theoretical and experimental data follow the same trends, notable differences can be observed in both plots. For example, no bronchial deposition has been found by Heyder et al. (1986) for particle diameters between 1 and 100 nm, while the IDEAL model predicts a substantial deposition fraction for this size range, consistent with the experimental data of Kim and Jaques (2000). For acinar deposition, model predictions are consistently lower than the experimental values. For comparison with other deposition models, the reader is referred to Fig. 12A (bronchial) and B (acinar), illustrating regional deposition fractions predicted by different lung deposition models (*note*: if these data were also included, Fig. 16 would become too crowded).

These differences between theoretical and experimental results might be partly caused by attributing particles initially deposited in the bronchioles to the acinar region because of the slow bronchial clearance in bronchioles (Hofmann & Sturm, 2004). The existence of a slow bronchial clearance phase has been documented in several retention measurements by Stahlhofen (1989), Stahlhofen et al. (1995), ICRP (1994), Smith et al. (2008) a few years after the measurements of Heyder et al. (1986) have been published. Assuming the size-dependence of the slow bronchial clearance fraction proposed by Hofman and Sturm (2004), "corrected" fractional depositions were computed for all particle sizes below about 6.5 μm, thereby reducing acinar deposition, while increasing bronchial deposition. The most dramatic change can be seen for particles below 2 μm, where the reassignment of deposition sites leads to deposition fractions consistent with the semi-experimental observations of Kim and Jaques (2000), where Heyder et al. (1986) could not detect any deposition.

The agreement between model predictions and "corrected" experimental data is much better as compared to the originally published data, though differences still do exist. However, considering (i) experimental uncertainties and intersubject variability, and (ii) the application of two different lung models in the analyses of Koblinger and Hofmann (1985), Kim and Hu (1998), and Kim and Jaques (2000), the agreement is quite acceptable.

6.3. *Local deposition in a group of successive airway generations*

Particle deposition within the bronchial and acinar compartments, i.e. in specific airway generations, cannot, at least at present, be obtained experimentally. However, there are two experimental approaches, which indirectly allow the experimental determination of deposition fractions in a group of successive airway generations: (i) the serial bolus dispersion technique, and (ii) the reconstruction of three-dimensional deposition patterns measured by Single Photon Emission Computed Tomography (SPECT). These deposition fractions may then be extrapolated to single airway generations by relating serial lung volumes to airway generations.

With the serial aerosol bolus technique a defined concentration of monodisperse particles is injected into the inhaled air at a predetermined point in time during the inhalation phase, forming a narrow aerosol bolus. As the aerosol bolus penetrates deeper into the lungs by a stepwise increase of the volumetric lung depth, i.e. by administering the bolus later during the inspiration time, the expired bolus is shifted towards later expiration times and its width increases, the latter termed "bolus dispersion" (Heyder et al., 1988; Brand et al., 1997; Darquenne et al., 1997; Sarangapani & Wexler, 1999). While the primary goal of Brand et al. (1997) was to investigate the dispersion of an exhaled bolus, with deposition only as a byproduct, Kim and Hu (1998) and Kim and Jaques (2000) used the same technique to specifically determine particle deposition throughout the thoracic airway generations of the lung.

The most comprehensive set of experimental data was published by Brand et al. (1997). who measured aerosol bolus dispersion and deposition in 79 healthy subjects. The comparison of bolus deposition data predicted by a specific version of the stochastic deposition model with these experimental data is depicted in Fig. 17 as a function of the volumetric depth reached by the front of the bolus (Hofmann et al., 2008). Although deposition refers here to a given sequence of airway generations corresponding to the selected volumetric lung depth, it suggests that current models correctly predict the distribution of deposition fractions among bronchial and alveolated airway generations (Hofmann et al., 2008; Choi & Kim, 2007).

Based on the measurement of three-dimensional distributions of radiolabelled aerosols by SPECT measurements, Fleming et al. (1995) developed a methodology to quantify measured three-dimensional distributions for comparison with predicted deposition fractions. At present, the limited spatial resolution of the SPECT technique does not allow a direct comparison between measured spatial activity distributions and simulated three-dimensional deposition patterns. Thus such a comparison is currently based on the conversion of the measured spatial activity distribution to deposition fractions in a series of 10 concentric, equidistant semi-spherical shells of the right lung (Fleming et al., 1995), thus no longer representing truly experimental data.

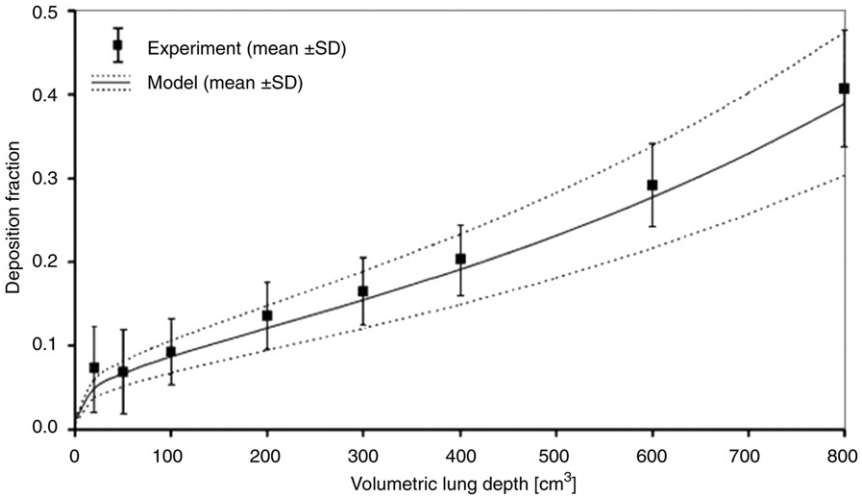

Fig. 17. Comparison of bolus deposition of 0.84 μm particles predicted by the stochastic deposition model IDEAL for specified oral breathing conditions (V_T=1000 ml, f=15 min^{-1}) with the experimental results of Brand et al. (1997) as a function of the volumetric depth (Hofmann et al., 2008).

Since the IDEAL deposition model contains information on the spatial arrangement of all airways, the spatial coordinates of a given deposition event can be assigned to a given shell. This allows the calculation of deposition fractions for all airway generations (Hofmann et al., 2005). An alternative approach was reported by Fleming et al. (2000), who converted the measured shell deposition data to deposition fractions in airway generations based on Weibel's (1963) model A. In general, both modelling predictions follow the general trend of the measured data, although some differences can be observed in the peripheral airways.

6.4. *Airway models and casts*

Physical airway models and airway casts can be used to check the applicability of analytical equations for various physical deposition mechanisms under well defined in-vitro inhalation conditions, primarily for inspiration only (Cohen & Asgharian, 1990; Martonen, 1983; Robinson et al., 2006). For obvious experimental reasons, they are restricted to the trachea and large bronchial airways. While earlier airway models were based on published morphometric lung models (Martonen, 1983; Cohen & Asgharian, 1990; Oldham et al., 1997), recent measurements utilize realistic human replica models (Li et al., 1998; Smith et al., 2001; Robinson et al., 2006).

Since airway models are composed of a series of straight cylindrical tubes, which usually refer to a specific morphometric lung model, experimental results as well as modelling predictions can be compared for the same airway geometry. Hence airway models allow the validation of physical deposition equations in single tubes and their extrapolation to a sequence of bifurcating airways. In contrast, airway casts offer the possibility to measure particle deposition in an anatomically realistic airway geometry. For example, Cohen and Asgharian (1990) derived semi-empirical equations for diffusional deposition in bronchial airways for conditions of developing flow.

In conclusion, measurements of particle deposition in airway models and airway casts are of limited use for model comparison, since the contribution of deposition fractions in large bronchial airways to total and regional deposition is relatively small. However, their primary importance is that they offer the possibility (i) to derive semi-empirical deposition equations for complex geometries, such as nasal and oral airways or bronchial airway bifurcations and (ii) to determine local deposition patterns within airway generations, which can be predicted by CFPD calculations.

7. Aerosol deposition at the local scale

Local deposition of inhaled aerosols, i.e. in small, defined units of the lung geometry, will be discussed here only in connection with particle deposition calculations for the whole lung. In other words, with regard to the ability of localized deposition models to contribute to the improvement of current whole lung deposition models, e.g. by providing more realistic fluid dynamics patterns and physical deposition equations. Moreover, this area of research has expanded substantially in recent years and thus would deserve a separate review.

Single airways are the smallest morphometric unit in whole lung deposition models for which particle deposition can be predicted. Since analytical deposition equations refer to deposition efficiencies in straight cylindrical tubes, they cannot, by definition, provide information on local inhomogeneities of particle deposition within an airway or an airway bifurcation, such as the formation of "hot spots" at carinal ridges (Báláshazy et al., 1999). These localized deposits may be of great significance

regarding potential health effects of inhaled particles, and may explain the observed site selectivity of bronchial carcinomas (Churg & Vedal, 1996).

Analytical solutions of the transport and deposition equations in airway bifurcations can only be obtained under the assumption of an idealized bifurcation geometry (contiguous system of straight tubes) and idealized flow profiles throughout the whole airway bifurcation. Thus the consideration of anatomically realistic airway bifurcations (Hegedüs et al., 2004; Heistracher & Hofmann, 1995) and realistic three-dimensional flow profiles (Balásházy, 1994; Comer et al., 2001a; Hofmann et al., 2001; Martonen et al., 1997; Zhang et al., 2001) requires the application of numerical Computational Fluid and Particle Dynamics (CFPD) techniques for the solution of the partial differential transport equations, which have become commercially available in recent years. Deposition patterns within a defined geometric unit are finally determined by the intersection of simulated particle trajectories with the surrounding wall surfaces.

Current CFPD models permit the prediction of realistic particle deposition fractions or efficiencies and localized patterns in a few selected geometric units of the human respiratory tract. At present, local scale models are restricted to defined localized geometries because of the complexity of the lung geometry. The computational methods employed in these anatomical structures are generally similar, using commercially available CFPD programme packages, based on finite differences, finite elements or

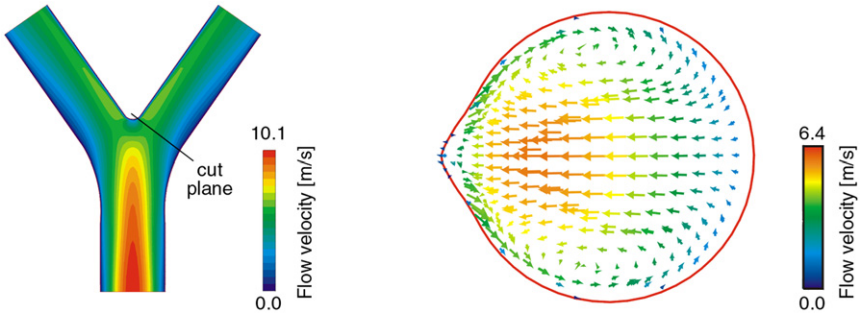

Fig. 18. Primary flow patterns during inspiration in a physiologically realistic central (generations 3–4) human airway bifurcation model (left) and secondary flows in the daughter branch downstream of the carinal ridge (right). The flow at the inlet of the parent branch refers to light physical activity breathing conditions (ICRP, 1994) with a laminar parabolic profile. The cut plane of the right panel is marked on the left panel (Balásházy et al., 2003).

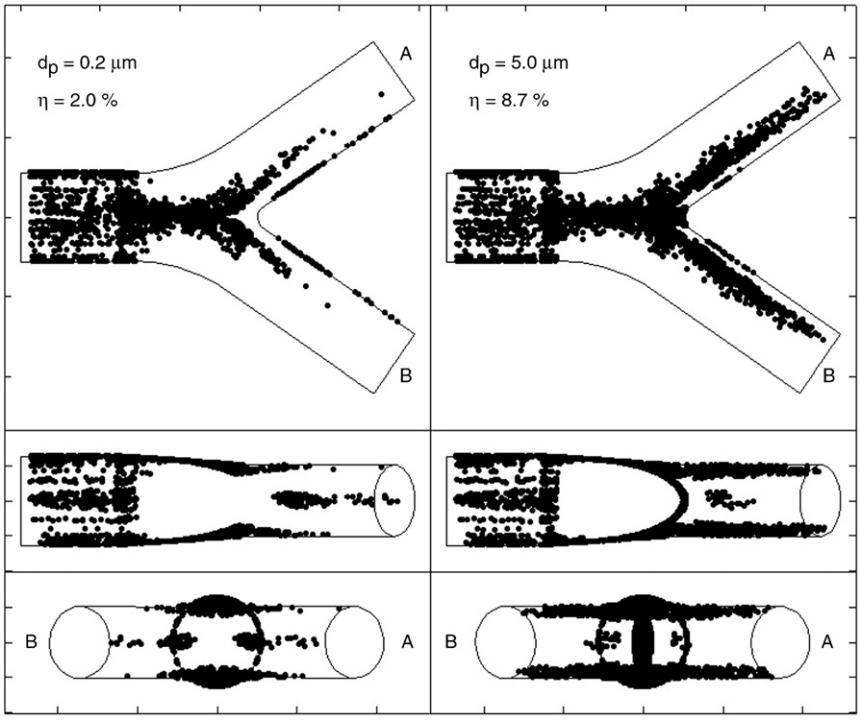

Fig. 19. Projected inspiratory spatial deposition patterns and related deposition efficiencies (η) of 0.2 and 5 µm unit density particles in a physiologically realistic central (generations 3–4) human airway bifurcation model, based on 100,000 randomly selected particles. The inlet flow refers to light physical activity breathing conditions (ICRP, 1994) with a laminar parabolic profile (Balásházy et al., 2003).

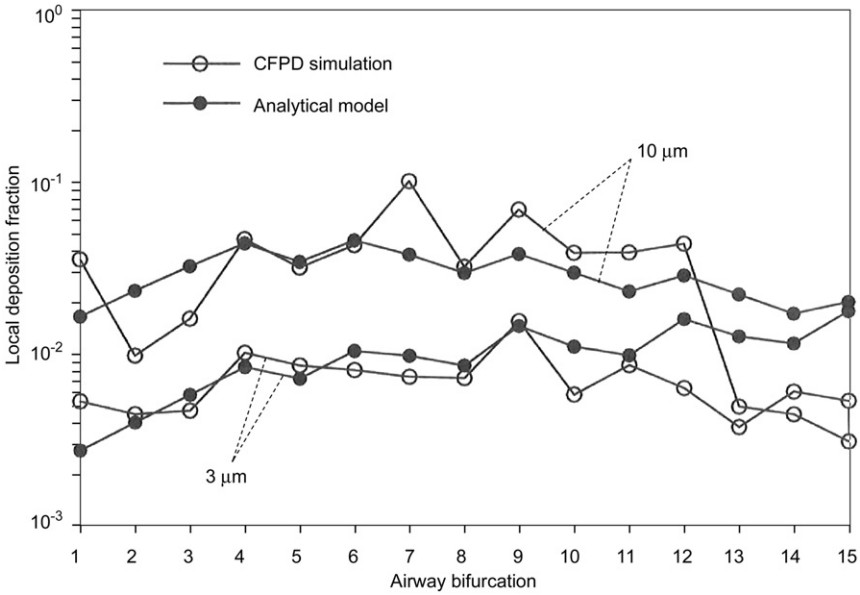

Fig. 20. Comparison of bifurcation by bifurcation deposition fractions of micrometre-sized particles during inspiration between CFPD simulations and analytical calculations for a flow rate of 30 l min^{-1} (Zhang et al., 2009).

finite volumes methods. Current CFPD models vary primarily with respect to the anatomical sites simulated and their morphological complexity, such as bronchial airway bifurcations, nasal and oral passages, and alveolated airways and alveoli.

A symmetric bifurcation is the simplest geometric unit of the airway system which requires already CFPD calculations. The effect of flow splitting at the carinal ridge, i.e. the dividing spur in the centre of the bifurcation, on resulting fluid dynamics patterns in the two daughter airways in the main plane of the bifurcation model, termed primary flow, and the formation of secondary flow patterns perpendicular to the axis of daughter airways are displayed in Fig. 18 (Balásházy et al., 2003).

In contrast to the idealized constant flow profiles assumed in whole lung models, a distinct spatial asymmetry of primary and secondary flows in both daughter airways can be observed. This asymmetry is further increased in asymmetric airway bifurcations and in multiple bifurcation models due to the branching asymmetry and the relative orientations of the bifurcation planes upon penetration into the lung.

Related particle deposition patterns in a single symmetric airway bifurcation model for generations 3–4 are exhibited in Fig. 19 for 200 nm and 5 µm unit density particles under light physical activity breathing conditions (ICRP, 1994). While the "hot spots" of deposited 5 µm particles at the carinal ridge can be explained by the dominant action of the inertial impaction mechanism, the preferential deposition of 200 nm particles at the same site is not consistent with the isotropic Brownian motion. This indicates that secondary flows and inverse flows directly above the carina (see Fig. 19) cause these inhomogeneous deposition patterns (Hofmann et al., 2001). Note that such secondary flows cannot be considered in whole lung models.

In summary, inspection of Fig. 18 (fluid dynamics) and 19 (particle deposition) reveals that airflow and particle deposition are strongly correlated, while they are assumed to be separated in analytical whole lung models.

As in the case of analytical whole lung models, there are also a few major limitations to the numerical local scale approach: (1) models cannot be validated by comparison with experimental in-vivo data at the corresponding anatomical level, e.g. in single airway bifurcations, particularly not the distribution of deposited particles, only in simplified airway models or casts. (2) At present, these models cannot be used to predict deposition in the whole lung during a complete breathing cycle because of the computational complexity and, even more importantly, because of the lack of morphometric data for all bronchial and acinar airways, which will not become available in the near future (*note*: current CT and MRI measurements are restricted to upper bronchial airways).

The strengths and limitations of analytical and numerical deposition models are illustrated in Fig. 20 for particle deposition in the tracheobronchial tree during steady inspiratory flow, where CFPD simulations are compared to analytical calculations (Zhang et al., 2009). This comparison reveals that both modelling approaches agree rather well with each other, despite some differences in individual bifurcations. In other words, complex numerical models predict the same regional deposition fractions as relatively simple analytical models, However, these numerical calculations could only be performed for a simplified symmetric, single path morphology of the bronchial airways, thereby neglecting the random variations of airway dimensions, branching and gravity angles. In other words, the apparent gain by the application of realistic flow and particle transport patterns is compensated by the loss of a realistic airway geometry. Only if all morphometric airway parameters are known, can the capabilities of numerical local scale models be fully exploited.

In addition, predictions of particle deposition in the whole lung would require corresponding numerical simulations for the alveolar region as well as for expiratory flows. Despite these limitations with respect to whole lung deposition, it must be emphasized that local scale models are indispensable to the prediction of local deposition and, consequently, local health effects, which cannot be predicted by current analytical whole lung models.

8. Current problems and future solutions

At present, the two major problems limiting the application of analytical whole lung models are (i) the intersubject variability of morphological and physiological parameters and related person-specific variations of deposition fractions, and (ii) the application of analytical deposition equations for straight cylindrical airways under specified flow conditions to airway bifurcations for realistic inspiratory and expiratory flow patterns.

Because of the observed significant intersubject variability of lung deposition, the prediction of particle deposition for individual subjects (“personalized deposition”), based on available morphometric and physiological measurements, would greatly improve the application of deposition models for toxicological and therapeutic purposes. Indeed, geometric standard deviations of deposition densities in bronchial airway bifurcations range from 2.1 to 3.8 (Hofmann et al., 2006). This intersubject variability limits the validity of any comparison between modelling predictions and experimental data.

Pulmonary function tests permit the determination of individual breathing patterns (tidal volume V_T and breathing frequency f) and of different lung volumes and capacities. Alternatively, V_T and FRC can be obtained by allometric equations as functions of body height and age (ICRP, 1994). Based on a given FRC, individual airway diameters and lengths can be derived by the application of scaling procedures, most commonly assuming a linear relationship. However, such scaling procedures can account for volumetric differences, but not for structural differences. Direct measurements of bronchial airway dimensions by CT and MRI techniques would allow an even more realistic determination of linear airway dimensions. In addition, the anatomical Fowler deadspace of the lung, representing the volume of nonalveolarized conductive airways, can be obtained by $C^{18}O_2$ single breath measurements (Möller et al., 2009).

The most significant practical value of numerical local scale models is the improvement of current analytical whole lung deposition models by providing more realistic deposition equations for complex geometries, such as nasal and oral regions, bronchial airway bifurcations and peripheral alveolated airways, considering the correlation between airflow and particle transport.

The structurally complex geometry of the extrathoracic region produces complex flow patterns and particle trajectories, including turbulences, secondary and jet-like flows. Because of this, only semi-empirical deposition equations could be obtained so far through mathematical fits to experimental data (e.g. Cheng, 2003; ICRP, 1994). However, the application of CFPD methods allows, for the first time, to derive deposition efficiencies from first principles (e.g. Farkas et al., 2006; Martonen et al., 2002, 2003; Matida et al., 2004; Shi et al., 2007; Zhang et al., 2002c).

Analytical deposition equations commonly refer to straight cylindrical tubes. Although no analytical equations are currently available for bronchial airway bifurcations, they can be predicted by numerical methods. For example, Worth Longest and Vinchukar (2009) recently proposed an equation for the branch-averaged deposition efficiency for inertial impaction in a double bifurcation during expiratory flow as a function of both Stokes and Dean numbers. For inspiratory deposition of inhaled nanoparticles for the whole tracheobronchial tree, consisting of 15 airway bifurcations (Weibel, 1963), Zhang et al. (2008) presented an equation for the bifurcation deposition efficiency as a function of the diffusion parameter Δ.

Likewise, the simulation of fluid dynamics patterns in expanding and contracting alveoli or in alveolar ducts and sacs (e.g. Tsuda et al., 1995, 2008, 2002; Darquenne & Paiva, 1996; Balásházy et al., 2008) can provide information on the mixing of the incoming tidal air with the residual air remaining in the lungs after the end of the preceding expiration phase.

9. Discussion and conclusions

An unavoidable source of uncertainty for any comparison between modelling predictions and experimental deposition data is the intersubject variability of airway dimensions and structural relationships. While the morphometric data of the stochastic lung model were derived from two specific lungs (Koblinger & Hofmann, 1985), they may have differed in the lungs of the volunteers participating in the deposition experiments used for model validation, e.g. Heyder et al. (1986), Schiller et al. (1988); Kim and Hu (1998), and Kim and Jaques (2000). Although intersubject differences in FRC can be accounted for by appropriate scaling procedures, structural differences cannot be determined by lung function tests. Likewise, the scaling of airway dimensions from TLC to standard FRC and from standard FRC to individual FRC cannot be verified by morphometric measurements.

As a result of the stochastic nature of the human airway system (Koblinger & Hofmann, 1985), deposition fractions exhibit significant statistical fluctuations, which are even exacerbated for deposition densities due to the correlation between deposition fractions and surface areas (Hofmann et al., 2006). This variability of deposition fractions and densities in human airway generations for a given aerosol concentration in the inhaled air poses a major challenge to the quest to find a causal relationship between local dose and resulting health effects in the lungs for individual people.

Calculations of particle deposition in the whole lung commonly refer to spherical particles and to specific morphometric lung models representing healthy, adult individuals. For consistency, all results presented in this paper

refer to such conditions. However, mechanisms have been indentified which modify lung morphology and/or the effective particle diameter, and hence also particle deposition, and this adds some uncertainty to general predictions. For example, the effective particle size upon inhalation can be changed due to hygroscopic growth or by coagulation, as discussed previously in Section 2.4.

Moreover, environmental and workplace aerosol particles are usually not ideal spheres, as is the case for most combustion generated aerosols which are heavily aggregated and often characterized by fractal dimensions below 2. Although the principal deposition mechanisms by diffusion and inertia can be modelled accurately when using the correct equivalent diameters (see Section 2.4), and although the relevant equivalent diameters are in principle captured by standard measurement techniques, the fractal nature of such particles does introduce additional uncertainties into model predictions. For example, fractal agglomerates may change their shape (and hence their deposition relevant size) at a high relative humidity; furthermore there is some evidence of an enhanced deposition by interception, which is not fully investigated at the time of writing of this review.

In case of truly fibrous or chain-like aerosols, the motion of a particle can no longer be described by an averaged orientation (and thus a unique mobility equivalent or aerodynamic diameter), because its orientation is affected by the flow field (e.g. Balásházy et al., 1990, 2005). The respective equivalent sizes of a very elongated particle change by about 20–25% for the aerodynamic diameter, and about 40–50% for the mobility equivalent diameter, depending on whether it moves parallel or perpendicular to its principal axis (Kasper & Shaw, 1983).

The major factors modifying the lung morphology of a healthy, adult person and related respiratory physiology are children's lungs and lung diseases. Except of the first years of life, as long as alveolization takes place, the lungs of children can be considered as a miniature version of the adult lung, i.e. measured adult lung dimensions can be scaled down to lung volumes at different ages (Hofmann, 1982a, 1982b; Phalen et al., 1985; Ménache et al., 2008). Corresponding age-specific reference values of breathing parameters for selected ages have been defined by ICRP (1994).

Several lung diseases affect the morphometry of the lung, such as asthma in the bronchial region, leading to a spasmodic constriction of bronchial airways (Martonen et al., 2003), emphysema in the acinar region, which causes the destruction of the alveolar architecture (Sturm & Hofmann, 2004), or chronic obstructive pulmonary disease (COPD), a more general term, which encompasses both effects.

In the present paper, size distributions and deposition fractions refer to the number of inhaled particles. Beside such number distributions, deposition models can also predict mass deposition (Subramaniam et al., 2003) or surface deposition (Alföldy et al., 2009), depending on the specific problem investigated.

Following the deposition event, particles are removed from their initial deposition sites by several clearance mechanisms, such as mucociliary clearance in bronchial and bronchiolar airways, or uptake by macrophages in alveolated airways (ICRP, 1994). In case of short-term inhalation, say a few minutes or hours, the number of insoluble particles in the lungs will continuously drop until all particles have left the lung (Hofmann & Asgharian, 2003). Since the deposited fraction of inhaled particles varies with time, this deposition behaviour may be termed "time-dependent deposition". In case of continuous inhalation over a longer period of time (long-term inhalation), say from a few days to years, a steady-state between deposition and clearance will be reached after some time. Thus a fraction of inhaled particles, commonly called the "retained fraction", will remain in the lungs during most of the exposure period.

Because of the ever increasing speed of computers and the availability of more sophisticated CFPD codes, one could envision a distant future, in which CFPD calculations could be performed for all airways from the entrance of the nose (or mouth) down to the alveoli for inspiration and back during expiration. While the technological progress may indeed accomplish this goal, the question must to be asked, whether such a goal would be a reasonable or desirable one. At present, such an approach is not meaningful, because the morphometric information necessary for these simulations will not be obtained in the near future at the required spatial resolution. Thus a system's approach based on the analytical approach seems to be most appropriate for the whole lung, while a CFPD approach is required for localized regions. However, CFPD calculations may aid the analytical whole lung approach by providing more realistic deposition efficiencies for bifurcating airways and contracting and expanding alveoli. In addition, simulations of chaotic mixing in alveoli and alveolated airways may allow the determination of realistic mixing factors between inhaled and residual air (Tsuda et al., 2008).

Acknowledgements

The author gratefully acknowledges the contributions of friends and colleagues to the development of analytical whole lung and numerical local scale models and to the preparation of this manuscript. In particular, the author is indebted to Renate Winkler-Heil, Bahman Asgharian, James Marsh, Risa Robinson and Chong Kim for providing theoretical predictions for specific particle sizes and breathing patterns, thus enabling model comparisons for the same input data.

References

Alföldy, B., Giechaskiel, B., Hofmann, W., & Drossinos, Y. (2009). Size-distribution dependent lung deposition of diesel exhaust particles. *Journal of Aerosol Science*, *40*, 652–663.

Altshuler, B. (1959). Calculation of regional deposition of aerosol in the respiratory tract. *Bulletin of Mathematical Biophysics*, *21*, 257–270.

Anjilvel, S., & Asgharian, B. (1995). A multiple-path model of particle deposition in the rat lung. *Fundamentals of Applied Toxicology*, *28*, 41–50.
Asgharian, B., Hofmann, W., & Bergmann, R. (2001). Particle deposition in a multiple-path model of the human lung. *Aerosol Science and Technology*, *34*, 332–339.
Asgharian, B., Price, O.T., & Hofmann, W. (2006). Prediction of particle deposition in the human lung using realistic models of lung ventilation. *Journal of Aerosol Science*, *37*, 1209–1221.
Balásházy, I. (1994). Simulation of particle trajectories in bifurcating tubes. *Journal of Computational Physics*, *110*, 11–22.
Balásházy, I., & Hofmann, W. (1993a). Particle deposition in airway bifurcations—I. Inspiratory flow. *Journal of Aerosol Science*, *24*, 745–772.
Balásházy, I., & Hofmann, W. (1993b). Particle deposition in airway bifurcations—II. Expiratory flow. *Journal of Aerosol Science*, *24*, 773–786.
Balásházy, I., Hofmann, W., Farkas, A., & Madas, B.G. (2008). Three-dimensional model for aerosol transport and deposition in expanding and contracting alveoli. *Inhalation Toxicology*, *20*, 611–621.
Balásházy, I., Hofmann, W., & Heistracher, T. (1999). Computation of local enhancement factors for the quantification of particle deposition patterns in airway bifurcations. *Journal of Aerosol Science*, *30*, 185–203.
Balásházy, I., Hofmann, W., & Heistracher, T. (2003). Local particle deposition patterns may play a key role in the development of lung cancer. *Journal of Applied Physiology*, 1719–1725.
Balásházy, I., Martonen, T.B., & Hofmann, W. (1990). Fiber deposition in airway bifurcations. *Journal of Aerosol Medicine*, *3*, 243–260.
Balásházy, I., Moustafa, M., Hofmann, W., Szöke, W., El Hussain, A., & Ahmed, A.R. (2005). Simulation of fiber deposition in bronchial airways. *Inhalation Toxicology*, *17*, 717–727.
Baron, P.A., & Willeke, K. (2005). *Aerosol Measurement: Principles, Techniques and Applications*. Wiley-Interscience: New York.
Beeckmans, J.M. (1965). The deposition of aerosols in the respiratory tract. I. Mathematical analysis and comparison with experimental data. *Canadian Journal of Physiology and Pharmacology*, *43*, 157–172.
Brand, P., Friemel, I., Meyer, T., Schulz, H., Heyder, J., & Häußinger, K. (2000). Total deposition of therapeutic particles during spontaneous and controlled inhalations. *Journal of Pharmaceutical Sciences*, *89*, 724–731.
Brand, P., Rieger, C., Schulz, H., Beinert, T., & Heyder, J. (1997). Aerosol bolus dispersion in healthy subjects. *European Respiratory Journal*, *10*, 460–467.
Butler, J.P., & Tsuda, A. (1997). Effect of convective stretching and folding on aerosol mixing in the deep lung, assessed by approximate entropy. *Journal of Applied Physiology*, *83*, 800–809.
Cai, F.S., & Yu, C.P. (1988). Inertial and interceptional deposition of spherical particles and fibers n a bifurcating airway. *Journal of Aerosol Science*, *19*, 679–688.
Chan, T.L., & Lippmann, M. (1980). Experimental measurements and empirical modelling of the regional deposition of inhaled particles in humans. *American Industrial Hygiene Association Journal*, *41*, 399–409.
Cheng, K.H., Cheng, Y.S., Yeh, H.C., Guilmette, R.A., Simpson, S.Q., Yang, Y., & Swift, D.L. (1996). In vivo measurements of nasal airway dimensions and ultrafine aerosol deposition in the human nasal and oral airways. *Journal of Aerosol Science*, *27*, 785–801.
Cheng, Y.S. (2003). Aerosol deposition in the extrathoracic region. *Aerosol Science and Technology*, *37*, 659–671.
Choi, J.-I., & Kim, C.S. (2007). Mathematical analysis of particle deposition in human lungs: An improved single path transport model. *Inhalation Toxicology*, *19*, 925–939.
Churg, A., & Vedal, S. (1996). Carinal and tubular airway particle concentration in the large airways of nonsmokers in the general population: Evidence for high particle concentration at airway carinas. *Occupational Environmental Medicine*, *53*, 553–558.
Cohen, B.S., & Asgharian, B. (1990). Deposition of ultrafine particles in the upper airways: An empirical analysis. *Journal of Aerosol Science*, *21*, 789–797.
Cohen, B.S., Sussmann, R.G., & Lippmann, M. (1990). Ultrafine particle deposition in a human tracheobronchial cast. *Aerosol Science and Technology*, *12*, 1082–1091.
Comer, J.K., Kleinstreuer, C., & Zhang, Z. (2001a). Flow structures and particle deposition patterns in double bifurcation airway models. Part I. Airflow fields. *Journal of Fluid Mechanics*, *435*, 25–54.
Comer, J.K., Kleinstreuer, C., & Zhang, Z. (2001b). Flow structures and particle deposition patterns in double bifurcation airway models. Part II. Aerosol transport and deposition. *Journal of Fluid Mechanics*, *435*, 55–80.
Cruz, J.C. (1991). A combined parallel and series distribution model of inspired inert gases. *Respiration Physiology*, *86*, 1–14.
Darquenne, C., & Paiva, M. (1996). Two- and three-dimensional simulations of aerosol transport and deposition in alveolar zone of human lung. *Journal of Applied Physiology*, *80*, 1401–1414.
Darquenne, C., Brand, P., Heyder, J., & Paiva, M. (1997). Aerosol dispersion in human lung: Comparison between numerical simulations and experiments for bolus tests. *Journal of Applied Physiology*, *83*, 966–974.
Darquenne, C., & Paiva, M. (1994). One-dimensional simulation of aerosol transport and deposition in the human lung. *Journal of Applied Physiology*, *77*, 2889–2898.
Egan, M.J., & Nixon, W. (1985). A model of aerosol deposition in the lung for use in inhalation dose assessments. *Radiation Protection Dosimetry*, *11*, 5–17.
Farkas, Á., & Balásházy, I. (2008). Quantification of particle deposition in a symmetrical tracheobronchial model geometry. *Computers in Biology and Medicine*, *38*, 508–518.
Farkas, Á., Balásházy, I., & Szöcs, K. (2006). Characterization of regional and local deposition of inhaled drugs in the respiratory system by computational fluid and particles dynamics methods. *Journal of Aerosol Medicine*, *19*, 329–343.
Ferron, G. (1977). The size of soluble aerosol particles as a function of the humidity of the air. Application to the human respiratory tract. *Journal of Aerosol Science*, *8*, 251–267.
Ferron, G., Karg, E., & Peter, J.E. (1993). Estimation of deposition of polydisperse hygroscopic aerosol in the human respiratory tract. *Journal of Aerosol Science*, *24*, 655–670.
Findeisen, W. (1935). Über das Absetzen kleiner in der Luft suspendierter Teilchen in der menschlichen Lunge bei der Atmung. *Pflügers Archiv für die gesamte Physiologie*, *236*, 367–379.
Finlay, W. (2001). *The Mechanics of Inhaled Pharmaceutical Aerosols: An Introduction*. Academic Press: New York.
Fleming, J.S., Conway, J., Holgate, S., Bailey, A.G., & Martonen, T.B. (2000). Comparison of methods for deriving aerosol deposition by airway generation from three-dimensional radionuclide imaging. *Journal of Aerosol Science*, *31*, 1251–1259.
Fleming, J.S., Nassim, M., Hashish, A.H., Bailey, A.G., Conway, J., Holgate, S., Halson, P., Moore, E., & Martonen, T.B. (1995). Description of pulmonary deposition of radiolabeled aerosol by airway generation using a conceptual three-dimensional model of lung morphology. *Journal of Aerosol Medicine*, *8*, 341–356.
Foord, N., Black, A., & Walsh, M. (1978). Regional deposition of 2.5–2.7 μm diameter inhaled particles in healthy, male non-smokers. *Journal of Aerosol Science*, *9*, 343–357.
Friedlander, S.K. (2000). *Smoke, Dust and Haze: Fundamentals of Aerosol Dynamics*. Oxford University Press: New York.
Fukuchi, Y., Cosio, M., Murphy, B., & Engel, L.A. (1980). Intraregional basis for sequential filling and emptying of the lung. *Respiration Physiology*, *41*, 253–266.
Garcia, G.J.M., Tewksbury, E.W., Wong, B.A., & Kombello, J.S. (2009). Interindividual variability in nasal filtration as a function of nasal cavity geometry. *Journal of Aerosol Medicine and Pulmonary Drug Delivery*, *22*, 139–155.
Gerrity, T.R., Lee, P.S., Hass, F.J., Marinelli, A., Werner, P., & Lourenco, R.V. (1979). Calculated deposition of inhaled particles in the airway generations of normal subjects. *Journal of Applied Physiology*, *47*, 867–873.
Goo, J.H., & Kim, C.S. (2003). Theoretical analysis of particle deposition in human lungs considering stochastic variations of airway morphology. *Journal of Aerosol Science*, *34*, 585–602.
Gradon, L., & Orlicki, D. (1990). Deposition of inhaled aerosol particles in a generation of the tracheobronchial tree. *Journal of Aerosol Science*, *21*, 3–19.

Grant, B.J.B., Jones, H.A., & Hughes, J.M.B. (1974). Sequence of regional filling during a tidal breath in man. *Journal of Applied Physiology*, *37*, 158–165.
Grgic, B., Finlay, W.H., Burnell, P.K.P., & Heenan, A.F. (2004). In vitro intersubject and intrasubject deposition measurements in realistic mouth-throat geometries. *Journal of Aerosol Science*, *35*, 1025–1040.
Haefeli-Bleuer, B., & Weibel, E. (1988). Morphometry of the human pulmonary acinus. *The Anatomical Record*, *220*, 401–414.
Hansen, J.E., & Ampaya, E.P. (1975). Human air space shapes, sizes, areas, and volumes. *Journal of Applied Physiology*, *38*, 990–995.
Hegedüs, C.J., Balásházy, I., & Farkas, A. (2004). Detailed mathematical description of the geometry of airway bifurcations. *Respiratory Physiology & Neurobiology*, *141*, 99–114.
Heistracher, T., & Hofmann, W. (1995). Physiologically realistic models of bronchial airway bifurcations. *Journal of Aerosol Science*, *26*, 497–509.
Heyder, J., Armbruster, L., Gebhart, J., Grein, E., & Stahlhofen, W. (1975). Total deposition of aerosol particles in the human respiratory tract for nose- and mouth-breathing. *Journal of Aerosol Science*, *6*, 311–328.
Heyder, J., Blanchard, J.D., Feldman, H.A., & Brain, J.D. (1988). Convective mixing in human respiratory tract: Estimates with aerosol boli. *Journal of Applied Physiology*, *64*, 1273–1278.
Heyder, J., Gebhart, J., Rudolf, G., Schiller, C.F., & Stahlhofen, W. (1986). Deposition of particles in the human respiratory tract in the size range 0.005–15 μm. *Journal of Aerosol Science*, *17*, 811–825.
Hiller, F.C., Mazumder, M.K., Wilson, J.D., McLeod, P.C., & Bone, R.C. (1962). Human respiratory tract deposition using multimodal aerosols. *Journal of Aerosol Science*, *13*, 337–343.
Hinds, W.C. (1999). *Aerosol Technology: Properties, Behavior, and Measurement of Airborne Particles*. Wiley-Interscience: New York.
Hofmann, W. (1982a). Dose calculations for the respiratory tract from inhaled natural radioactive nuclides as a function of age—Part II: Basal cell dose distributions and associated lung cancer risk. *Health Physics*, *43*, 31–44.
Hofmann, W. (1982b). Mathematical model for the postnatal growth of the human lung. *Respiration Physiology*, *49*, 115–129.
Hofmann, W., & Asgharian, B. (2003). The effect of lung structure on mucociliary clearance and particle retention in human and rat lungs. *Toxicological Science*, *73*, 448–456.
Hofmann, W., Asgharian, B., & Winkler-Heil, R. (2002). Modeling intersubject variability of particle deposition in human lungs. *Journal of Aerosol Science*, *33*, 219–235.
Hofmann, W., Balásházy, I., & Heistracher, T. (2001). The relationship between secondary flows and particle deposition patterns. *Aerosol Science and Technology*, *35*, 958–968.
Hofmann, W., & Bergmann, R. (1998). Predictions of particle deposition patterns in human and rat airways. *Inhalation Toxicology*, *10*, 557–583.
Hofmann, W., & Koblinger, L. (1990). Monte Carlo modelling of aerosol deposition in human lungs. Part II: Deposition fractions and their sensitivity to parameter variations. *Journal of Aerosol Science*, *21*, 675–688.
Hofmann, W., & Koblinger, L. (1992). Monte Carlo modelling of aerosol deposition in human lungs. Part III: Comparison with experimental data. *Journal of Aerosol Science*, *23*, 51–63.
Hofmann, W., Martonen, T.B., & Graham, R.C. (1989). Predicted deposition of nonhygroscopic aerosols in the human lung as a function of subject age. *Journal of Aerosol Medicine*, *2*, 49–68.
Hofmann, W., Morawska, L., Winkler-Heil, R., & Moustafa, M. (2009). Deposition of combustion aerosols in the human respiratory tract: Comparison of theoretical predictions with experimental data considering nonspherical shape. *Inhalation Toxicology*, *21*, 1154–1164.
Hofmann, W., Pawlak, E., & Sturm, R. (2008). Semi-empirical stochastic model of aerosol bolus dispersion in the human lung. *Inhalation Toxicology*, *20*, 1059–1073.
Hofmann, W., & Sturm, R. (2004). Stochastic model of particle clearance in human bronchial airways. *Journal of Aerosol Medicine*, *17*, 73–89.
Hofmann, W. Sturm, R., & Ahmed, M. (2003), Modeling ultrafine particle deposition and clearance in the human respiratory tract. In *15th International Technion Symposium on Particulate Matter and Health*. Vienna: Technion Society, pp. 57–65.
Hofmann, W., Sturm, R., Fleming, J.S., Conway, J.H., & Bolt, L. (2005). Simulation of three-dimensional particle deposition patterns in human lungs and comparison with experimental SPECT data. *Aerosol Science and Technology*, *39*, 771–781.
Hofmann, W., Winkler-Heil, R., & Balásházy, I. (2006). The effect of morphological variability on surface deposition densities of inhaled particles in human bronchial and acinar airways. *Inhalation Toxicology*, *18*, 809–819.
Horsfield, K., & Cumming, G. (1968). Morphology of the bronchial tree in man. *Journal of Applied Physiology*, *24*, 373–383.
Igarashi, Y., Yamakawa, A., Kim, C.K., & Ikeda, N. (1987). Distribution of uranium in human lungs. *Radioisotopes*, *36*, 501–504.
Ingham, D.B. (1975). Diffusion of aerosols from a stream flowing through a cylindrical tube. *Journal of Aerosol Science*, *6*, 125–132.
Ingham, D.B. (1984). Deposition of aerosol from a stream flowing through a short cylindrical pipe. *Journal of Aerosol Science*, *15*, 637–641.
International Commission on Radiological Protection (ICRP). (1994). *Human Respiratory Tract Model for Radiological Protection. ICRP Publication 66*, Annals of ICRP 24, Nos. 1–3. Oxford: Pergamon Press.
James, A.C. (1988). Lung dosimetry. In W.W. Nazaroff & A.V. Nero (Eds.), *Radon and Its Decay Products in Indoor Air*. John Wiley & Sons: New York, pp. 259–309.
Kasper, G. (1982a). Dynamics and measurements of smokes, I—Size characterization of nonspherical particles. *Aerosol Science & Technology*, *1*, 187–199.
Kasper, G. (1982b). Dynamics and measurements of smokes, II—Aerodynamic diameter of chain aggregates in the transition regime. *Aerosol Science & Technology*, *1*, 201–215.
Kasper, G., & Shaw, D.T. (1983). Comparative size distribution measurements on chain aggregates. *Aerosol Science & Technology*, *2*, 369–381.
Kasper, G., & Wen, H.Y. (1984). Dynamics and measurements of smokes, IV—Comparative measurements on submicron chain aggregates with an aerosol centrifuge and an aerodynamic particle sizer APS 33. *Aerosol Science & Technology*, *3*, 405–409.
Kesavanathan, J., & Swift, D.L. (1998). Human nasal passage particle deposition: The effect of particle size, flow rate, and anatomical factors. *Aerosol Science and Technology*, *28*, 457–463.
Kim, C.S., & Fisher, D.M. (1999). Deposition characteristics of aerosol particles in sequentially bifurcating airway models. *Aerosol Science and Technology*, *31*, 198–220.
Kim, C.S., Fisher, D.M., Lutz, D.J., & Gerrity, D.R. (1994). Particle deposition in bifurcating airway models with varying airway geometry. *Journal of Aerosol Science*, *25*, 567–581.
Kim, C.S., & Hu, S.C. (1998). Regional deposition of inhaled particles in human lungs: Comparison between men and women. *Journal of Applied Physiology*, *84*, 1834–1844.
Kim, C.S., & Iglesias, A.J. (1989). Deposition of inhaled particles in bifurcating airway models: Inspiratory deposition. *Journal of Aerosol Medicine*, *2*, 1–14.
Kim, C.S., & Jaques, P.A. (2000). Respiratory dose of inhaled ultrafine particles in healthy adults. *Philosophical Transactions of the Royal Society London A*, *358*, 2693–2705.
Kim, C.S., & Jaques, P.A. (2004). Analysis of total respiratory deposition of inhaled ultrafine particles in adult subjects at various breathing patterns. *Aerosol Science and Technology*, *38*, 525–540.
Koblinger, L., & Hofmann, W. (1985). Analysis of human lung morphometric data for stochastic aerosol deposition calculations. *Physics in Medicine and Biology*, *30*, 541–556.
Koblinger, L., & Hofmann, W. (1990). Monte Carlo modelling of aerosol deposition in human lungs. Part I: Simulation of particle transport in a stochastic lung structure. *Journal of Aerosol Science*, *21*, 661–674.
Landahl, H.D. (1950). On the removal of airborne droplets by the human respiratory tract. I. The lung. *Bulletin of Mathematical Biophysics*, *23*, 43–56.
Lazaridis, M., Broday, D.M., Hov, O., & Georgopoulos, P.G. (2001). Integrated exposure and Dose modeling and analysis system. 3. Deposition of inhaled particles in the human respiratory tract. *Environmental Science and Technology*, *35*, 3727–3734.
Lee, D.Y., & Lee, J.W. (2001). Dispersion during exhalation of an aerosol bolus in a double bifurcation. *Journal of Aerosol Science*, *32*, 805–815.

Lee, J.W., Lee, D.Y., & Kim, W.S. (2000). Dispersion of an aerosol bolus in a double bifurcation. *Journal of Aerosol Science*, *31*, 491–505.
Li, W., Xiong, J.Q., & Cohen, B.S. (1998). The deposition of unattached radon progeny in a tracheobronchial cast as measured with iodine vapour. *Aerosol Science and Technology*, *28*, 502–510.
Martonen, T.B. (1982). Analytical model of hygroscopic particle behavior in human airways. *Bulletin of Mathematical Biology*, *44*, 425–442.
Martonen, T.B. (1983). Measurement of particle dose distribution in a model of a human larynx and tracheobronchial tree. *Journal of Aerosol Science*, *14*, 11–22.
Martonen, T.B. (1993). A mathematical model for the selective deposition of inhaled pharmaceuticals. *Journal of Pharmaceutical Sciences*, *82*, 1191–1199.
Martonen, T.B., Barnett, A.E., & Miller, F.J. (1985). Ambient sulphate aerosol deposition in man: Modeling the influence of hygroscopicity. *Environmental Health Perspectives*, *63*, 11–24.
Martonen, T.B., Graham, R.C., & Hofmann, W. (1989). Human subject age and activity level: Factors addressed in a biomathematical deposition program for extrapolation modeling. *Health Physics*, *57*(Suppl. 1), 49–59.
Martonen, T.B., Quan, L., Zhang, Z., & Musante, C.J. (2002). Flow simulation in the human upper human respiratory tract. *Cell Biochemistry and Biophysics*, *37*, 27–36.
Martonen, T.B., Zhang, Z., & Musante, C.J. (2003). Fine particle deposition within human nasal airways. *Inhalation Toxicology*, *15*, 283–303.
Martonen, T.B., Zhang, Z., & Yang, Y. (1997). Particle diffusion from developing flows in rough-walled tubes. *Aerosol Science and Technology*, *26*, 1–11.
Matida, E.A., Finlay, W.H., Lange, C.F., & Grgic, B. (2004). Improved numerical simulation of aerosol deposition in an idealized mouth-throat. *Journal of Aerosol Science*, *35*, 1–19.
Melandri, C., Tarroni, G., Prodi, V., De Zaiacomo, T., Formignani, M., & Lombardi, C.C. (1983). Deposition of charged particles in the human airways. *Journal of Aerosol Science*, *14*, 184–186.
Ménache, M.G., Hofmann, W., Asgharian, B., & Miller, F.J. (2008). Airway geometry: Models of children's lungs for use in dosimetry modeling. *Inhalation Toxicology*, *20*, 101–126.
Milic-Emili, J., Henderson, J.A.M., Dolovich, M.B., Trop, T., & Kaneko, K. (1966). Regional distribution of inspired gas in the lung. *Journal of Applied Physiology*, *21*, 749–759.
Mitsakou, C., Helmis, C., & Housiadas, C. (2005). Eulerian modelling of lung deposition with sectional representation of aerosol dynamics. *Journal of Aerosol Science*, *36*, 75–94.
Möller, W., Meyer, G., Scheuch, G., Kreyling, W., & Bennett, W.D. (2009). Left-to-right asymmetry of aerosol deposition after shallow bolus inhalation depends on lung ventilation. *Journal of Aerosol Medicine and Pulmonary Drug Delivery*, *22*, 333–339.
National Commission of Radiological Protection (NCRP). (1997). Deposition, Retention and Dosimetry of Inhaled Radioactive Substances. *NCRP Report No. 125*. National Council on Radioprotection and Measurements. NCRP, Bethesda, MD.
Nixon, W., & Egan, M.J. (1987). Modelling study of regional deposition of inhaled aerosol with special reference to effects of ventilation asymmetry. *Journal of Aerosol Science*, *18*, 563–579.
Oldham, M.J., Mannix, R.C., & Phalen, R.F. (1997). Deposition of monodisperse particles in hollow models representing adult and child-size tracheobronchial airways. *Health Physics*, *72*, 827–834.
Park, K., Kittelson, D.B., & McMurry, P.H. (2004). Structural properties of diesel exhaust particles measured by transmission electron microscopy (TEM): Relationship between particle mass and mobility. *Aerosol Science and Technology*, *38*, 881–889.
Parkash, O. (1977). Lung cancer. A statistical study based on autopsy data from 1928–1972. *Respiration*, *34*, 295–304.
Phalen, R.F., Cuddihy, R.G., Fisher, G.L., Moss, O.R., Schlesinger, R.B., Swift, D.L., & Yeh, H.C. (1991). Main features of the proposed NCRP respiratory tract model. *Radiation Protection Dosimetry*, *38*, 179–184.
Phalen, R.F., Oldham, M.J., Beaucage, C.B., Crocker, T.T., & Mortensen, J.D. (1985). Postnatal enlargement of human tracheobronchial airways and implications for particle deposition. *The Anatomical Record*, *212*, 368–380.
Pich, J. (1972). Theory of gravitational deposition of particles from laminar flow in channels. *Journal of Aerosol Science*, *3*, 351–361.
Pityn, P., Chamberlain, M.J., King, M.E., & Morgan, W.K. (1995). Differences in particle deposition between the two lungs. *Respiratory Medicine*, *89*, 15–19.
Raabe, O.G., Yeh, H.C., Schum, G.M., & Phalen, R.F. (1976). Tracheobronchial Geometry: Human, Dog, Rat, Hamster. *Lovelace Foundation Report LF-53*. Albuquerque, NM: Lovelace Foundation.
Reist, P.C. (1993). *Aerosol Science and Technology*. McGraw-Hill: New York.
Robinson, R.J., Oldham, M.J., Clinkenbeard, R.E., & Rai, P. (2006). Experimental and numerical smoke deposition in a multi-generation human replica tracheobronchial model. *Annals of Biomedical Engineering*, *34*, 373–383.
Robinson, R.J., & Yu, C.P. (1998). Theoretical analysis of hygroscopic growth rate of mainstream and sidestream cigarette smoke particles in the human respiratory tract. *Aerosol Science and Technology*, *28*, 21–32.
Robinson, R.J., & Yu, C.P. (1999). Coagulation of cigarette smoke particles. *Journal of Aerosol Science*, *30*, 533–548.
Robinson, R.J., & Yu, C.P. (2001). Deposition of cigarette smoke particles in the human respiratory tract. *Aerosol Science and Technology*, *34*, 202–215.
Rudolf, G., Gebhart, J., Heyder, J., Schiller, C.F., & Stahlhofen, W. (1986). An empirical formula describing aerosol deposition in man for any particle size. *Journal of Aerosol Science*, *17*, 350–355.
Rudolf, G., Köbrich, R., & Stahlhofen, W. (1990). Modelling and algebraic formulation of regional aerosol deposition in man. *Journal of Aerosol Science*, *21*(Suppl. 1), S403–S406.
Rudolf, G., Köbrich, R., Stahlhofen, W., & James, A.C. (1994). Regional airway deposition in man—a statistical and algebraic model. *Annals of Occupational Hygiene*, *38*(Suppl. 1), 1–14.
Sarangapani, R., & Wexler, A.S. (1999). Modeling aerosol bolus dispersion in human airways. *Journal of Aerosol Science*, *30*, 1345–1362.
Scheckman, J.H., & McMurray, P.H. (2011). Deposition of silica agglomerates in a cast of human lung airways: Enhancement relative to spheres of equal mobility and aerodynamic diameter. *Journal of Aerosol Science*, *42*, 508–516.
Scherer, P.W., Shendalman, L.H., Green, N.M., & Bouhuys, A. (1975). Measurement of axial diffusivities in a model of the bronchial airways. *Journal of Applied Physiology*, *38*, 719–723.
Schiller, C.F., Gebhart, J., Heyder, J., Rudolf, G., & Stahlhofen, W. (1988). Deposition of monodisperse insoluble aerosol particles in the 0.005–0.2 μm size range within the human respiratory tract. *Annals of Occupational Hygiene*(Suppl. 1), 41–49.
Shi, H., Kleinstreuer, C., & Zhang, Z. (2007). Modeling of inertial particle transport and deposition in human nasal cavities with wall roughness. *Journal of Aerosol Science*, *38*, 398–419.
Smith, J.R.H., Bailey, M.R., Etherington, G., Shutt, A.L., & Youngman, M.J. (2008). Effect of particle size on slow particle clearance from the bronchial tree. *Experimental Lung Research*, *34*, 287–312.
Smith, S., Cheng, Y.S., & Yeh, H.C. (2001). Deposition of ultrafine particles in human tracheobronchial airways of adults and children. *Aerosol Science and Technology*, *35*, 697–709.
Stahlhofen, W. (1989). Human lung clearance following bolus inhalation of radioaerosols. In J.D. Crapo, E.D. Smolko, F.J. Miller, J.A. Graham, & A.W. Hayes (Eds.), *Extrapolation of Dosimetric Relationships for Inhaled Particles and Gases*. Academic Press: San Diego, pp. 153–166.
Stahlhofen, W., Gebhart, J., & Heyder, J. (1980). Experimental determination of the regional deposition of aerosol particles in the human respiratory tract. *American Industrial Hygiene Association Journal*, *41*, 385–398.
Stahlhofen, W., Rudolf, G., & James, A.C. (1989). Intercomparison of experimental regional aerosol deposition data. *Journal of Aerosol Medicine*, *2*, 285–308.
Stahlhofen, W., Scheuch, G., & Bailey, M.R. (1995). Investigations of retention of inhaled in the human bronchial tree. *Radiation Protection Dosimetry*, *60*, 311–319.
Sturm, R., & Hofmann, W. (2004). Stochastic simulation of alveolar particle deposition in lungs affected by different types of emphysema. *Journal of Aerosol Medicine*, *17*, 357–372.

Subramaniam, R.P., Asgharian, B., Freijer, J.I., Miller, F.J., & Anjilvel, S. (2003). Analysis of lobar differences in particle deposition in the human lung. *Inhalation Toxicology*, *15*, 1–21.
Takano, N., Nishida, N., Itoh, M., Hyo, N., & Mayima, Y. (2006). Inhaled particle deposition in unsteady-state respiratory flow at a numerically constructed model of the human larynx. *Journal of Aerosol Medicine*, *19*, 314–328.
Taulbee, D.B., & Yu, C.P. (1975). A theory of aerosol deposition in the human respiratory tract. *Journal of Applied Physiology*, *38*, 77–85.
Taulbee, D.B., Yu, C.P., & Heyder, J. (1978). Aerosol transport in the human lung from analysis of single breaths. *Journal of Applied Physiology*, *44*, 803–812.
Tippe, A., & Tsuda, A. (1999). Recirculating flow in an expanding alveolar model: Experimental evidence of flow-induced mixing of aerosol in the pulmonary acinus. *Journal of Aerosol Science*, *31*, 979–986.
Tsuda, A., Henry, F.S., & Butler, J.P. (1995). Chaotic mixing of alveolated duct flow in rhythmically expanding pulmonary acinus. *Journal of Applied Physiology*, *79*, 1055–1063.
Tsuda, A., Henry, F.S., & Butler, J.P. (2008). Gas and erosol mixing in the acinus. *Journal of Respiratory Physiology & Neurobiology*, *163*, 139–149.
Tsuda, A., Rogers, R.A., Hydon, P.E., & Butler, J.P. (2002). Chaotic mixing deep in the lung. *Proceedings of the National Academy of Sciences USA*, *99*, 10173–10178.
Tu, K.W., & Knutson, E.O. (1984). Total deposition of ultrafine hydrophobic and ygroscopic erosol in the human respiratory system. *Aerosol Science and Technology*, *3*, 453–465.
Veeze, P. (1986). *Rationale and Methods of Early Detection in Lung Cancer*. Van Gorcum: Assen, NL.
Wang, C.S. (1975). Gravitational deposition of particles from laminar flows in inclined channels. *Journal of Aerosol Science*, *6*, 191–204.
Weibel, E.R. (1963). *The Morphometry of the Human Lung*. Academic Press: New York.
Wen, H.Y., & Kasper, G. (1984). Dynamics and measurements of smokes, III—Drag and orientation of chain aggregates in an electrical mobility spectrometer. *Aerosol Science & Technology*, *3*, 397–403.
Williams, M.M.R., & Loyalka, S.K. (2000). *Aerosol Science: Theory and Practice*. Wiley-Interscience: New York.
Winkler-Heil, R., & Hofmann, W. (2009). Inter- and intra-lobar deposition of inhaled particles. In *Proceedings of the European Aerosol Conference 2009*, Karlsruhe, Abstract T101A01.
Yeh, H.C., & Schum, G.M. (1980). Models of the human lung airways and their application to inhaled particle deposition. *Bulletin of Mathematical Biology*, *42*, 461–480.
Yu, C.P., & Cohen, B.S. (1994). Tracheobronchial airway deposition. *Annals of Occupational Hygiene*, *38*(Suppl. 1), 83–89.
Yu, C.P., & Diu, C.K. (1982). A probabilistic model for intersubject deposition variability of inhaled particles. *Aerosol Science and Technology*, *1*, 335–362.
Yu, C.P., Nicolaides, P., & Soong, T.T. (1979). Effect of random airway sizes on aerosol deposition. *American Industrial Hygiene Association Journal*, *40*, 999–1005.
Zhang, L., Asgharian, B., & Anjilvel, S. (1997). Inertial deposition of particles in the human upper airway system. *Aerosol Science and Technology*, *26*, 97–110.
Zhang, Z., & Kleinstreuer, C. (2002). Transient airflow structures and particle transport in a sequentially branching lung airway model. *Physics of Fluids*, *14*, 862–880.
Zhang, Z., Kleinstreuer, C., & Kim, C.S. (2001). Flow structure and particle transport in a triple bifurcation model. *Journal of Fluids Engineering*, *123*, 320–330.
Zhang, Z., Kleinstreuer, C., & Kim, C.S. (2002a). Computational analysis of micron-particle deposition in a human triple bifurcation airway model. *Computational Methods in Biomechanical and Biomedical Engineering*, *5*, 135–147.
Zhang, Z., Kleinstreuer, C., & Kim, C.S. (2002b). Aerosol deposition efficiencies and upstream release positions for different inhalation models in an upper bronchial airway model. *Aerosol Science and Technology*, *36*, 828–844.
Zhang, Z., Kleinstreuer, C., & Kim, C.S. (2002c). Micro-particle transport and deposition in a human oral airway model. *Journal of Aerosol Science*, *33*, 1635–1652.
Zhang, Z., Kleinstreuer, C., & Kim, C.S. (2008). Airflow and nanoparticle deposition in a 16-generation tracheobronchial airway model. *Annals of Biomedical Engineering*, *36*, 2095–2110.
Zhang, Z., Kleinstreuer, C., & Kim, C.S. (2009). Comparison of analytical and CFD models with regard to micron particle deposition in a human 16-generation tracheobronchial airway model. *Journal of Aerosol Science*, *40*, 16–28.